Diagnostics evaluation of flow dependent B-matrix (LAM background error correlations)- 4th draft

Maria Monteiro*

January 16, 2009

Contents

1 Introduction **2**

2 J_b diagnostics **2**

3 Experimental work **7**

4 Presentation of results **11**
4.1 Seasonal statistics 11
4.2 Daily statistics: a case-study 12

5 Remarks and conclusions **13**

A Seasonal statistics **20**
A.1 Total variance 20
A.1.1 Horizontal averaged standard deviation profiles - each network 20
A.2 Horizontal auto-correlations 24
A.2.1 Vertical profiles of horizontal length-scale - each network 24
A.2.2 Variance spectra - each network 28
A.3 Vertical auto-correlations 32
A.4 Cross-covariances and percentages of explained variance 48

*Instituto de Meteorologia, Lisbon, Portugal

B Daily statistics **48**
B.1 Total variance 48
B.1.1 Time evolution of averaged std at levels 850hPa and 500hPa - each network 49
B.2 Horizontal auto-correlations 57
B.2.1 Time evolution of horizontal length-scale at levels 850hPa and 500hPa - all networks 57
B.2.2 Time evolution of horizontal length-scale at levels 850hPa and 500hPa - each network 58

C Daily analyse **66**

1 Introduction

The basic achievement of the work here decribed was the analyse of flow dependent background error statistics of a Limited Area Model (LAM) estimated by the Ensemble Method. The background error statistics were plotted during two different seasonal periods, in order to track the daily and seasonal influence of meteorological phenomena. Besides, the robustness of the Ensemble Method to estimate such statistics had to be examined in order to overseen its impact once used on the operational reference data assimilation scheme. A generic ensemble data assimilation system was set up for this particular task using the 3D-var methodology on the ALADIN/France model. This work was supervised by Loïk Berre and followed by Claude Fischer. The work here decribed was performed during a Summer stay at Métèo-France in accordance with the 2008 ALADIN project working plan and supported by the project flat-rate budget. It was also supported by the Portuguese service where part of the experiments were remotely concluded thanks to the facilities early provided by the OLIVE team and it should allow the author to get in touch with ensemble techniques applied to data assimilation sciences.

2 J_b diagnostics

It is quite easy to show, under some simplifying hypotesis, that the equations which describe the error evolution of a reference data assimilation system are exactly the same which describe the dispersion error evolution of an ensemble data assimilation system, if the gain matrix $\mathbf{K}$ remains the same in both systems [3]. This suggests that the dispersion error of an ensemble data assimilation system can be a good approximation of the real background error

used by the analytical data assimilation method.

In fact, looking into detail the Figure 1 and taking into account the equations of both the analysis (1) and the forecast steps (2),

$$\mathbf{x}^a_{i+1} = \mathbf{x}^b_{i+1} + \mathbf{K}(\mathbf{y} - \mathbf{H}\mathbf{x}^b_{i+1}) \tag{1}$$

$$\mathbf{x}^b_{i+1} = \mathbf{M}\mathbf{x}^a_i \tag{2}$$

we arrive to the following error evolution equations for the analysis and forecast steps, (3) and (4),

$$e^a_{i+1} = e^b_{i+1} + \mathbf{K}(\mathbf{y} - \mathbf{H}e^b_{i+1}) \tag{3}$$

$$e^b_{i+1} = \mathbf{M}e^a_i + e^m_{i+1} \tag{4}$$

where, $\mathbf{K} = \mathbf{B}\mathbf{H}^\mathbf{T}(\mathbf{H}\mathbf{B}\mathbf{H}^\mathbf{T} + \mathbf{R})^{-\mathbf{1}}$ is the gain matrix, $\mathbf{B}$ is the spatial covariance matrix of background errors, $\mathbf{R}$ is the spatial covariance matrix of observation errors and $\mathbf{H}$ is the observation operator that transforms a model state vector into the observations vector.

As usual on the former equations we represent the analysis field valid at the instant $t_{i+1} = t_i + 6h$ by $\mathbf{x}^a_{i+1}$, while $\mathbf{x}^b_{i+1}$ represents the forecast field at the same instant. Moreover, $\mathbf{M}$ is the operator that corresponds to the $6h$ integration provided by the forecast model and $\mathbf{y}$ is the observation vector. Furthermore, e^a_{i+1} represents the analysis error when producing the analysis field valid at instant $t_{i+1} = t_i + 6h$ and e^b_{i+1} represents the forecast error when producing the forecast field $\mathbf{x}^b_{i+1}$ valid at instant $t_{i+1} = t_i + 6h$.

Considering the analysis equation (1) for two different sets of observations it is possible to demonstrate that the dispersion between the ensemble members of our ensemble data assimilation system simulates the analysis and forecast errors of the forecast system, such that

$$\epsilon^a_{i+1} = \epsilon^b_{i+1} + \mathbf{K}(\mathbf{y} - \mathbf{H}\epsilon^b_{i+1}) \tag{5}$$

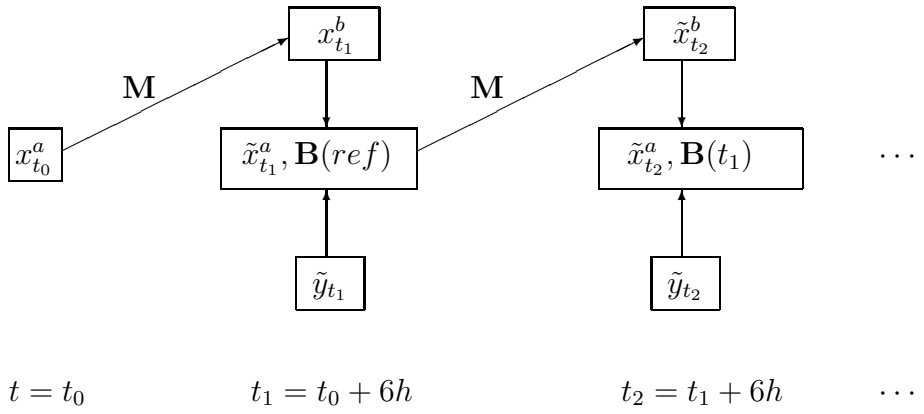

Figure 1: Schematic illustration of the data assimilation cycle which is replicated by the N members of the data assimilation ensemble used.

$$\epsilon^b_{i+1} = \mathbf{M}\epsilon^a_{i+1} + \epsilon^m_{i+1} \tag{6}$$

due to the fact that $\mathbf{K}$ is the same matrix as in the analysis step equation, where ϵ^a_{i+1} corresponds to the differences on their analysis valid at instant $t_{i+1} = t_i + 6h$ and ϵ^b_{i+1} corresponds to the differences on their forecast fields production valid at the same instant.

The 3-dimensional variational data assimilation problem in ALADIN, requires the minimization of a cost function J defined by

$$J = J_b + J_o = \frac{1}{2}(\mathbf{x} - \mathbf{x}^b)^T\mathbf{B}^{-1}(\mathbf{x} - \mathbf{x}^b) + \frac{1}{2}(\mathbf{Hx} - \mathbf{y})^T\mathbf{R}^{-1}(\mathbf{Hx} - \mathbf{y}) \tag{7}$$

Here J_b measures the distance to a background model state $\mathbf{x}^b$ and J_o measures the distance to the vector $\mathbf{y}$ of the observations; $(...)^T$ denotes the transposed matrix and the remaining mathematical symbols keep their previous meaning.

Ideally, the analysis cost function should be specified in terms of fields

which have the same resolution as the forecast model. However, this makes the cost function computationally expensive to minimize. The incremental formulation reduces computational expense by minimizing a cost function which has a lower resolution than is used by the forecast model [5]. This is a reasonable approach because the analysis increments are generally rather smooth, at least with current methods for specifying background error correlations. The cost function for the incremental formulation is then defined as follows:

$$J = J_b + J_o = \frac{1}{2}\delta\mathbf{x}'^T\mathbf{B}'^{-1}\delta\mathbf{x}' + \frac{1}{2}(H\mathbf{x}^b + \mathbf{H}'\delta\mathbf{x}' - \mathbf{y})^T\mathbf{R}^{-1}(H\mathbf{x}^b + \mathbf{H}'\delta\mathbf{x}' - \mathbf{y}) \tag{8}$$

The model background field $\mathbf{x}^b$ is provided at full model resolution, while the assimilation increment $\delta\mathbf{x}'$ is provided at another, in general lower, spatial resolution. In this formulation the full non-linear observation operator H for the background field $\mathbf{x}^b$ is used, instead of the linearized observation operator $\mathbf{H}'$, applied to the increment $\delta\mathbf{x}'$. The background error covariance matrix $\mathbf{B}'$ now has squared dimension of the assimilation increment.

According with Fischer *et al.* (2006) [4] the ALADIN variational code benefited initially from the original incremental formulation introduced in global assmilation and Berre (2000) presented the formulation of the background-error covariance matrix as the counterpart of the global, spherical harmonic formulation.

Using the assumptions of homogeneity and isotropy of background error covariances as well as assuming the non-separability of these statistical structures in spectral space Berre (2000) shown that, for instance, for specific humidity forecast errors at levels z, z' the covariance between two spectral coefficients could be written as

$$\overline{q^z_{mn} q^{z'}_{mn}{}^*} = \sigma_z \sigma'_z \sqrt{\gamma_z(k^*)\gamma'_z(k^*)} r_{k^*}(z, z') \tag{9}$$

where σ_z, σ'_z are the average standard-deviations of levels z, z', γ_z, γ'_z are the normalized spectral densities of the variance at those levels and $r_{k^*}(z, z')$ is the vertical correlation between levels z, z' for the total wave number k^* [2].

In practice, the determination of the analysis field by our reference system, $\mathbf{x}_a$, is not straigthforward since it requires the numerical inversion of the $\mathbf{B}$ matrix (or in fact, to the inversion of $\mathbf{B}'$ see equation 8) which has a huge dimension. Therefore the solution of the practical analysis problem is found through the choice of an appropriate set of variables which make this matrix a block-diagonal one, the so-called control variables and which usage requires in turn the pre-determination of forecast error statistics by use of empirical data in a process completely separated from the original reference data assimilation system. In fact, this formalism which is expressed below, uses the linear balance relationship between the two sets of variables to invert a system whose operators are block-diagonal matrices representing homogeneous and isotropic auto-covariance and cross-covariance statistcs in the spectral space, using the assumption of non-separability of the statistical structures between vertical and horizontal scales of the forecast errors:

$$\begin{aligned} \zeta &= \zeta && (10)\\ \eta &= \mathcal{M}\mathcal{H}\zeta + \eta_u && (11)\\ (T, P_s) &= \mathcal{N}\mathcal{H}\zeta + \mathcal{P}\eta_u + (T, P_s)_u && (12)\\ q &= \mathcal{Q}\mathcal{H}\zeta + \mathcal{R}\eta_u + \mathcal{S}(T, P_s)_u + q_u && (13) \end{aligned}$$

where $(\zeta, \eta, (T, P_s), q)$ are the model variables consisting on the vorticity, the divergence, the mass and the specific humidity and $(\zeta, \eta_u, (T, P_s)_u, q_u)$ is the set of control variables where $(\cdots)_u$ represents the unbalanced parts of the correspondent model variables. $\mathcal{H}$ is called the horizontal balance operator which is a diagonal matrix that transforms spectral coefficients of vorticity into those of balanced balanced geopotential, P_b; $\mathcal{M}, \mathcal{N}$ and $\mathcal{P}$ are the so-called vertical balance operators, which are block-diagonal matrices relating vertical profiles of control (or predictors) with those of the model (or predictands) variables.

As it was said previously, these statistical structures have to be computed outside the assimilation scheme using empirical data in order to be available during the cost function minimization.

On the date of elaboration of the heredescribed work, the statistical structures of background errors (our 6h forecast errors) on the ALADIN/France data assimilation system were fully determined by climatological processes.

However, it is now quite known that the forecast errors are induced not only by the inaccuracies of the model equations but also by the propagation of the initial state errors according with the degree of the flow predictability. Therefore it is expected that the coupling between the statistics of forecast errors of the different model variables should be strongly linked to the local meteorological features. Therefore the idea of using daily statistics has become a natural step hence a methodology to optimal filter the statistical noise when using the ensemble-based background-error variances to estimate those structures was scientifically justified [6]. This fact justifies the goal of this work to diagnose, before using them on the operational data assimilation system, the new statistical structures estimates.

Several diagnostics were proposed for such analysis that were prepared and analysed according with the description done on the next sections.

3 Experimental work

To procede with the required analyse of the background errors statistics to be used on ALADIN/France operacional data assimilation system, the sequence of ensemble data assimilation experiments described on Table 1 have been executed.

Two different experimental periods have been considered, both of one month long: a Winter period, starting on the 11th of February 2008 at 18UTC (in fact the first cycle of the ensemble is just to pick up the initial and boundary conditions from the ARPEGE deterministic run so it is not considered meaningful for the study we do) and a Summer period which started on the 2th of July 2008 at 18UTC. For these two time periods both the seasonal and the daily statistics have been determined. Besides, to confirm for the robustness of the ensemble method when simulating the background errors, two data assimilation ensembles have been considered for each season period where different "seeds" for the observations perturbation generation were introduced. On Table 1 such ensembles are characterised.

Averaged vertical correlations for the model variables, as well as vertical profiles and spectra for different model and statistical parameters have been performed using $festat$ and $fediacov$ applications under OLIVE[1] using a full month set of data to calculate the monthly statistics and the daily results

[1]Outil de Lancement Interactif et de Visualisation d'Experiences

Table 1: Data assimilation ensemble experiments characteristics

expid	*period*	*seed*	*statistics*	"*coupling*"	remarks
B0KN	20080212–20080313	member	daily femars	62FK	73NZ varbc
B0KQ	20080212–20080313	–	daily festat	B0KN	lstabal=.false.
B0KT	20080212–20080313	–	daily fediacov	B0KQ	
B0LE	20080212	–	month. festat	B0KN	lstabal=.true.
B0LM	20080212	–	month. fediacov	B0LE	
B0L4	20080212–20080313	n+member	daily femars	62WO	73NZ varbc
B0L8	20080212–20080313	–	daily festat	B0L4	lstabal=.false.
B0L9	20080212–20080313	–	daily fediacov	B0L8	
B0MB	20080212	–	month. festat	B0L4	lstabal=.true.
B0MC	20080212	–	month. fediacov	B0MB	
B0LG	20080703–20080804	member	daily femars	62FK	oper varbc
B0LC	20080703–20080804	–	daily festat	B0LG	lstabal=.false.
B0LD	20080703–20080804	–	daily fediacov	B0LC	
B0MD	20080703	–	month. festat	B0LG	lstabal=.true.
B0ME	20080703	–	month. fediacov	B0MD	
B0MF	20080703–20080804	n+member	daily femars	62WI	oper varbc
B0MG	20080703–20080704	–	daily festat	B0MF	lstabal=.false.
B0MH	20080703–20080704	–	daily fediacov	B0MG	
B0MI	20080703	–	month. festat	B0MF	lstabal=.true.
B0MJ	20080703	–	month. fediacov	B0MI	

to have the daily statistics. Moreover, time series of those parameters have been created whose plots have been examined for the required meteorological analyses. Technical guidance on the usage of the tools used to create the plots is left on this section.

To plot the vertical correlations of the model parameters on the spectral space, the following tools have been used according with the description:

1. *run_get_files*

   get_diacov_files gets by ftp all the 2008 fediacov files from cougar experiment's which name is given as input argument. Exact number of days to be used on the experiment and exact number of ensemble of members have to be known in advance, whatever the real number of days already available from the experiment

2. *run_plot_statistics*

   plot_vertical_correlations plots the statistics coming from fediacov files. In particular, plots the averaged vertical correlations of model variables for each experiment which name is known in advance.

   magxy.f

To plot the vertical profiles and spectra of the different model and statistical parameters, one script has been used, that call several procedures (Korn and GNU scripts) according with the following description:

1. *run_get_files*

   get_diacov_files gets by ftp all the 2008 fediacov files from cougar experiment's which name is given as input argument. Exact number of days to be used on the experiment and exact number of ensemble of members have to be known in advance, whatever the real number of days already available from the experiment

2. *run_plot_statistics*

   plot_lsc_comp plots the vertical profiles for horizontal characteristic length scales of the background error, for two experiments on the same plot allowing its comparison. The names of the experiments are input arguments

plot_std_comp plots the vertical profiles for horizontally averaged standard deviations of the background error, for two experiments on the same plot allowing its comparison. The names of the experiments are input arguments

plot_var_comp plots the varance spectra of background errors fro two experiments on the same plot, allowing its comparison. The names of the experiments are input arguments

plot_std plots the vertical profiles of standard deviations backgroung errors using the results of a single experiment. The name of the experiment is given as input argument

To plot the time series, three scripts have been sequentially used which call different procedures (Korn or GNU scripts or then FORTRAN programs) according with the following description:

1. *run_get_files*

   get_diacov_files gets by ftp all the 2008 fediacov files from cougar experiment's which name is given as input argument. Exact number of days to be used on the experiment and exact number of ensemble of members have to be known in advance, whatever the real number of days already available from the experiment

2. *run_time_series*

   series.f90 prepares individual time series for each experiment first day of the experiment has to be known in advance

3. *run_time_series_all_network*

   series_all.f90 prepares individual time series for each experiment first day of the experiment has to be known in advance. The difference for *series.f90* is that this time all the hour cycles are considered on the same time series

4. *run_plot_series*

   plot_series plots the time series, one on each plot, for a fixed number of model and statistic parameters. time series are plotted for whatever available number of days

   plot_series_comp plots the time series, two by each plot allowing appropriate comparison, for a fixed number of model and statistic parameters. time series are plotted for whatever available number of days

4 Presentation of results

In order to allow a clear view of the results, its presentation and analyse is done into two different sections, one dedicated to seasonal statistics and one dedicated to daily statistics. The results are illustrated on the graphics organized in two appended sections: the Appendix A for the seasonal statistics and the Appendix B for the daily statistics. Along those graphics, the Winter ensemble results are introduced as "Ens1" and "Ens2" while the two Summer ensemble results are pointed as "Ens3" and "Ens4".

4.1 Seasonal statistics

The profiles of horizontally averaged standard deviation (avstd) of the error background for the model variables of temperature, specific humidity, vorticity and divergence, obtained with data coming from the two experiment periods are shown on Figures 2, 3, 4 and 5. Main aspects are:

1. the robustness of the ensemble method: the effects on the results due to the differences on the pertubations generation for each ensemble inside the two sets are negligible compared with differences in season. On the way around the spread in each ensemble is meaningful enough to express the atmospheric structure variability.

2. as a general tendency, we can see that the results reflect the main aspects of the atmosphere structure: the background error avstd diminuishes for all the model parameters, since a few meters from the surface and up to model level 10 (10hPa). For the specific humidity the decrease of avstd on the levels above the planetary boundary layer (more precisely, up to 850hPa) - PBL - and up to around 250hPa where it disappears, is related to the moister decrease, in comparison with its magnitude inside the mixing layer. What concerns the vorticity, we can see that below the PBL its behaviour must be prescribed by the lower levels mixing phenomena, maitaining with a sligthly decrease up to around 500hPa its value from where it has shown a strong decrease due to the geostrophy of the free atmosphere movement except around level 25 where the jet stream is felt. For the divergence, similar comments can be drawn as for the vorticity.

3. seasonal differences on the two sets of ensembles are mainly visible for specific humidity, but also on the vorticity and on the divergence. Due to a higher heating of earth surface during the Summer period, we can expect to have an increase of background errors on the humidity

because the contents of moister on the PBL are also higher in magnitude during Winter period. The same can be said about vorticity and divergence.

4. the diurnal cycle is also visible trhough these graphics. All the profiles shown for the different daily runs match well in shape and values, for each the model parameters being the most relevant differences below model level 50 in the boundary layer, where the mixing phenomena, much dependent on the diurnal cycle of surface heating is governing: from 00UTC to 18UTC, we can see that stability of the lower part of atmosphere is destroyed, more visible during the Summer period due to the existence of higher surface temperatures, being the vorticity the parameter that shows more changes whithin the different networks, below 500hPa.

The horizontally averaged length-scales of horizontal auto-correlations are illustrated on Figures 6, 7, 8 and 9. These statistics indicate how fast the correlation function decreases away from the observation point. As a main aspect we can say that the vertical profiles of typical horizontal length-scales of correlations increase in high, showing that bigger wave length phenomena - synoptic - lead the spread of information at the highest levels.

The variance spectra graphics are another disgnostic of the simulated background errors, shown on Figures 10, 11, 12 and 13. Main aspect on this set of images were only the spectra for 500 is shown is that the values match well with those presented by [1]. As expected, during Summer there is a shift towards smaller scales (bigger wave numbers).

Finally for this first set of graphics the vertical auto-correlations for model levels are presented on Figures 14, 15, 16, 17, 18, 19, 20, 21, 22, 23, 24, 25, 26, 27, 28 and 29. Main aspects are:

1. differences between vertical correlations of different seasonal experiments are more meaningful than between two experiments on the same season.

2. broader vertical correlations in Summer than in Winter and the diurnal broadening of vertical correlations in Summer for specific humidity.

4.2 Daily statistics: a case-study

Along this report, the two Winter and the two Summer experiments results are appreciated simultaneously. Joinning on the same plot the results from

the each two seasonal ensemble sets give a perception of how much is the Ensemble method robust as an estimation method of the background error. Basic conclusions taken on the previous section help to learn from these statistics.

By observation of the time series, the Figures 30, 32, 34, 36 and 31, 33, 35, 37 for standard deviations (std) at 850 and 500 hPa and Figures 38, 40, 42 and 44, 39, 41, 43, 45 for horizontally averaged length-scales, we realise once again that the ensembles inside each season set show much consistent results.

To illustrate the expected flow dependency of these structures, a case study is considered for the Winter period. During this period, the flutuations of the background error standard deviation estimates are somehow modulated by a low frequency phenomena, showing two relative minima around days 4 and 22 of our Winter period experiment, respectively the 15th of February and the 04th of March 2008. In this section we try to understand if there is some match with meteorological phenomena.

On the 15th of February, there is a highly predictable situation over ALADIN/France domain (see Figure 46): a meteorological strongly stable and long scale situation prescribed by a deep high pressure system was located on the North of France territory. Humidity was then low at upper levels as well as vorticity and divergence. Looking to the daily statistics, both the time series of std and of horizontal length-scale, we can then justify the low values of std together with quite high values of the length-scale, in opposition to what has happened on the 4th of March. On the 4th of March (see Figure 47) low values of humidity std are not associated with low values of vorticity and divergence std anylonger however, according with the length-scales, these parameters seem to be related to much shorter scales phenomena which is meteorologically justified by the presence of the instabilities generated by the upper level through.

5 Remarks and conclusions

As expected, the ensemble runs appear o provide robust estimations of seasonal and daily variations of error covariances. These results will be deepened in a forthcoming scientific paper.

References

[1] Abdelhak, Razagui and Berre, Loïk. Calcul de covariances d'érreur d'ébauche pour de 3d-var aladin l60. *GMAP Internal Report*, 2007.

[2] Berre, Loïk. Estimation of synoptic and mesoscale forecast error covariances in a limited area model. *Monthly Weather Review*, 128:644–667, 2000.

[3] Gérald Desroziers, Loïk Berre, Olivier Pannekoucke, Simona Ştefănescu, Pierre Brousseau, Ludovic Auger, Bernad Chapnik, and Laure Raynaud. Flow-dependent error covariances from variational assimilation ensembles on global and regional domains. *unknown*, 2008.

[4] Fischer, Claude and Montmerle, Thibaut and Berre, Loïk and Auger, Ludovic and Stefanescu, Simona Ecaterina. An overview of the variational assimilation in the aladin/france numerical weather-prediction system. *Q. J. R. Meteorolo. Soc*, 131:3477–3492, 2006.

[5] Fisher, Mike. Assimilation techniques (3): 3dvar. In ECMWF, editor, *Meteorological Training Course Lecture Series*. ECMWF, 2002.

[6] Raynaud, Laure and Berre, Loïk and Desroziers, Gérald. Optimal filtering of ensemble-based background-error variances. *Q. J. R. Meteorolo. Soc*, 2007.

List of Figures

1 Schematic illustration of the data assimilation cycle which is replicated by the N members of the data assimilation ensemble used. 4

2 Horizontal averaged std values at 00UTC: temperature (top left; K), specific humidity (top right; kg kg-1), vorticity (bottom left; Jkg-1s) and divergence (bottom rigth; s-1); Y-axis: model levels 20

3 Horizontal averaged std values at 06UTC: temperature (top left; K), specific humidity (top right; kg kg-1), vorticity (bottom left; Jkg-1s) and divergence (bottom rigth; s-1); Y-axis: model levels 21

4 Horizontal averaged std values at 12UTC: temperature (top left; K), specific humidity (top right; kg kg-1), vorticity (bottom left; Jkg-1) and divergence (bottom rigth; s-1); Y-axis: model levels 22

5 Horizontal averaged std values at 18UTC: temperature (top left; K), specific humidity (top right; kg kg-1), vorticity (bottom left; Jkg-1) and divergence (bottom rigth; s-1); Y-axis: model levels 23

6 Horizontal averaged length-scale values at 00UTC: temperature (top left; K), specific humidity (top right; kg kg-1), vorticity (bottom left; Jkg-1 s) and divergence (bottom rigth; s-1); Y-axis: model levels 24

7 Horizontal averaged length-scale values at 06UTC: temperature (top left; K), specific humidity (top right; kg kg-1), vorticity (bottom left; Jkg-1 s) and divergence (bottom rigth; s-1); Y-axis: model levels 25

8 Horizontal averaged length-scale values at 12UTC: temperature (top left; K), specific humidity (top right; kg kg-1), vorticity (bottom left; Jkg-1 s) and divergence (bottom rigth; s-1); Y-axis: model levels 26

9 Horizontal averaged length-scale values at 18UTC: temperature (top left; K), specific humidity (top right; kg kg-1), vorticity (bottom left; Jkg-1 s) and divergence (bottom rigth; s-1); Y-axis: model levels 27

10 Averaged variance spectra values at 00UTC: temperature (top left; K), specific humidity (top right; kg kg-1), vorticity (bottom left; Jkg-1 s) and divergence (bottom rigth; s-1); X-axis: wave number 28

11 Averaged variance spectra values at 06UTC: temperature (top left; K), specific humidity (top right; kg kg-1), vorticity (bottom left; Jkg-1 s) and divergence (bottom rigth; s-1); X-axis: wave number 29
12 Averaged variance spectra values at 12UTC: temperature (top left; K), specific humidity (top right; kg kg-1), vorticity (bottom left; Jkg-1 s) and divergence (bottom rigth; s-1); X-axis: wave number 30
13 Averaged variance spectra values at 18UTC: temperature (top left; K), specific humidity (top right; kg kg-1), vorticity (bottom left; Jkg-1 s) and divergence (bottom rigth; s-1); X-axis: wave number 31
14 Vertical auto-correlations values for temperature at 00UTC: 1rst Winter ens (top left), 2nd Winter ens (top right), 1rst Summer ens (bottom left) and 2nd Summer ens (bottom rigth) 32
15 Vertical auto-correlations values for temperature at 06UTC: 1rst Winter ens (top left), 2nd Winter ens (top right), 1rst Summer ens (bottom left) and 2nd Summer ens (bottom rigth) 33
16 Vertical auto-correlations values for temperature at 12UTC: 1rst Winter ens (top left), 2nd Winter ens (top right), 1rst Summer ens (bottom left) and 2nd Summer ens (bottom rigth) 34
17 Vertical auto-correlations values for temperature at 18UTC: 1rst Winter ens (top left), 2nd Winter ens (top right), 1rst Summer ens (bottom left) and 2nd Summer ens (bottom rigth) 35
18 Vertical auto-correlation values for specific humidity at 00UTC: 1rst Winter ens (top left), 2nd Winter ens (top right), 1rst Summer ens (bottom left) and 2nd Summer ens (bottom rigth) 36
19 Vertical auto-correlation values for specific humidity at 06UTC: 1rst Winter ens (top left), 2nd Winter ens (top right), 1rst Summer ens (bottom left) and 2nd Summer ens (bottom rigth) 37
20 Vertical auto-correlation values for specific humidity at 12UTC: 1rst Winter ens (top left), 2nd Winter ens (top right), 1rst Summer ens (bottom left) and 2nd Summer ens (bottom rigth) 38
21 Vertical auto-correlation values for specific humidity at 18UTC: 1rst Winter ens (top left), 2nd Winter ens (top right), 1rst Summer ens (bottom left) and 2nd Summer ens (bottom rigth) 39
22 Vertical auto-correlation values for divergence at 00UTC: 1rst Winter ens (top left), 2nd Winter ens (top right), 1rst Summer ens (bottom left) and 2nd Summer ens (bottom rigth) 40

23 Vertical auto-correlation values for divergence at 06UTC: 1rst Winter ens (top left), 2nd Winter ens (top right), 1rst Summer ens (bottom left) and 2nd Summer ens (bottom rigth) 41
24 Vertical auto-correlation values for divergence at 12UTC: 1rst Winter ens (top left), 2nd Winter ens (top right), 1rst Summer ens (bottom left) and 2nd Summer ens (bottom rigth) 42
25 Vertical auto-correlation values for divergence at 18UTC: 1rst Winter ens (top left), 2nd Winter ens (top right), 1rst Summer ens (bottom left) and 2nd Summer ens (bottom rigth) 43
26 Vertical auto-correlation values for vorticity at 00UTC: 1rst Winter ens (top left), 2nd Winter ens (top right), 1rst Summer ens (bottom left) and 2nd Summer ens (bottom rigth) 44
27 Vertical auto-correlation values for vorticity at 06UTC: 1rst Winter ens (top left), 2nd Winter ens (top right), 1rst Summer ens (bottom left) and 2nd Summer ens (bottom rigth) 45
28 Vertical auto-correlation values for vorticity at 12UTC: 1rst Winter ens (top left), 2nd Winter ens (top right), 1rst Summer ens (bottom left) and 2nd Summer ens (bottom rigth) 46
29 Vertical auto-correlation values for vorticity at 18UTC: 1rst Winter ens (top left), 2nd Winter ens (top right), 1rst Summer ens (bottom left) and 2nd Summer ens (bottom rigth) 47
30 Time evolution of the averaged error background std for 850hPa at 00UTC: temperature (top left; K), specific humidity (top right; kg kg-1), vorticity (bottom left; Jkg-1 s) and divergence (bottom rigth; s-1); X-axis: number of run days 49
31 Time evolution of the averaged error background std for 500hPa at 00UTC: temperature (top left; K), specific humidity (top right; kg kg-1), vorticity (bottom left; Jkg-1 s) and divergence (bottom rigth; s-1); X-axis: number of run days 50
32 Time evolution of the averaged error background std for 850hPa at 06UTC: temperature (top left; K), specific humidity (top right; kg kg-1), vorticity (bottom left; Jkg-1 s) and divergence (bottom rigth; s-1); X-axis: number of run days) 51
33 Time evolution of the averaged error background std for 500hPa at 06UTC: temperature (top left), specific humidity (top right), vorticity (bottom left; Jkg-1 s) and divergence (bottom rigth; s-1); X-axis: number of run days) 52
34 Time evolution of the averaged error background for 500hPa at 12UTC: temperature (top left; K), specific humidity (top right; kg kg-1), vorticity (bottom left; Jkg-1 s) and divergence (bottom rigth; s-1); X-axis: number of run days) 53

35 Time evolution of the averaged error background for 850hPa at 12UTC: temperature (top left; K), specific humidity (top right; kg kg-1), vorticity (bottom left; Jkg-1 s) and divergence (bottom rigth; s-1); X-axis: number of run days) 54
36 Time evolution of the averaged error background std for 850hPa at 18UTC: temperature (top left; K), specific humidity (top right; kg kg-1), vorticity (bottom left; Jkg-1 s) and divergence (bottom rigth; s-1); X-axis: number of run days) 55
37 Time evolution of the averaged error background std for 500hPa at 18UTC: temperature (top left; K), specific humidity (top right; kg kg-1), vorticity (bottom left; Jkg-1 s) and divergence (bottom rigth; s-1); X-axis: number of run days) 56
38 Time evolution of horizontal length-scale for 850hPa at 00UTC: temperature (top left; K), specific humidity (top right; kg kg-1), vorticity (bottom left; Jkg-1 s) and divergence (bottom rigth; s-1); X-axis: number of run days) 58
39 Time evolution of horizontal length-scale for 500hPa at 00UTC: temperature (top left; K), specific humidity (top right; kg kg-1), vorticity (bottom left; Jkg-1 s) and divergence (bottom rigth; s-1); X-axis: number of run days) 59
40 Time evolution of horizontal length-scale for 850hPa at 06UTC: temperature (top left; K), specific humidity (top right; kg kg-1), vorticity (bottom left; Jkg-1 s) and divergence (bottom rigth; s-1); X-axis: number of run days) 60
41 Time evolution of horizontal length-scale for 500hPa at 06UTC: temperature (top left; K), specific humidity (top right; kg kg-1), vorticity (bottom left; Jkg-1 s) and divergence (bottom rigth; s-1); X-axis: number of run days) 61
42 Time evolution of horizontal length-scale for 850hPa at 12UTC: temperature (top left; K), specific humidity (top right; kg kg-1), vorticity (bottom left; Jkg-1 s) and divergence (bottom rigth; s-1); X-axis: number of run days) 62
43 Time evolution of horizontal length-scale for 500hPa at 12UTC: temperature (top left; K), specific humidity (top right; kg kg-1), vorticity (bottom left; Jkg-1 s) and divergence (bottom rigth; s-1); X-axis: number of run days) 63
44 Time evolution of horizontal length-scale for 850hPa at 18UTC: temperature (top left; K), specific humidity (top right; kg kg-1), vorticity (bottom left; Jkg-1 s) and divergence (bottom rigth; s-1); X-axis: number of run days) 64

45 Time evolution of horizontal length-scale for 500hPa at 18UTC: temperature (top left; K), specific humidity (top right; kg kg-1), vorticity (bottom left; Jkg-1 s) and divergence (bottom rigth; s-1); X-axis: number of run days) 65
46 Analyse of the flow on the 15th February 2008 67
47 Analyse of the flow on the 4th March 2008 68

A Seasonal statistics

A.1 Total variance

A.1.1 Horizontal averaged standard deviation profiles - each network

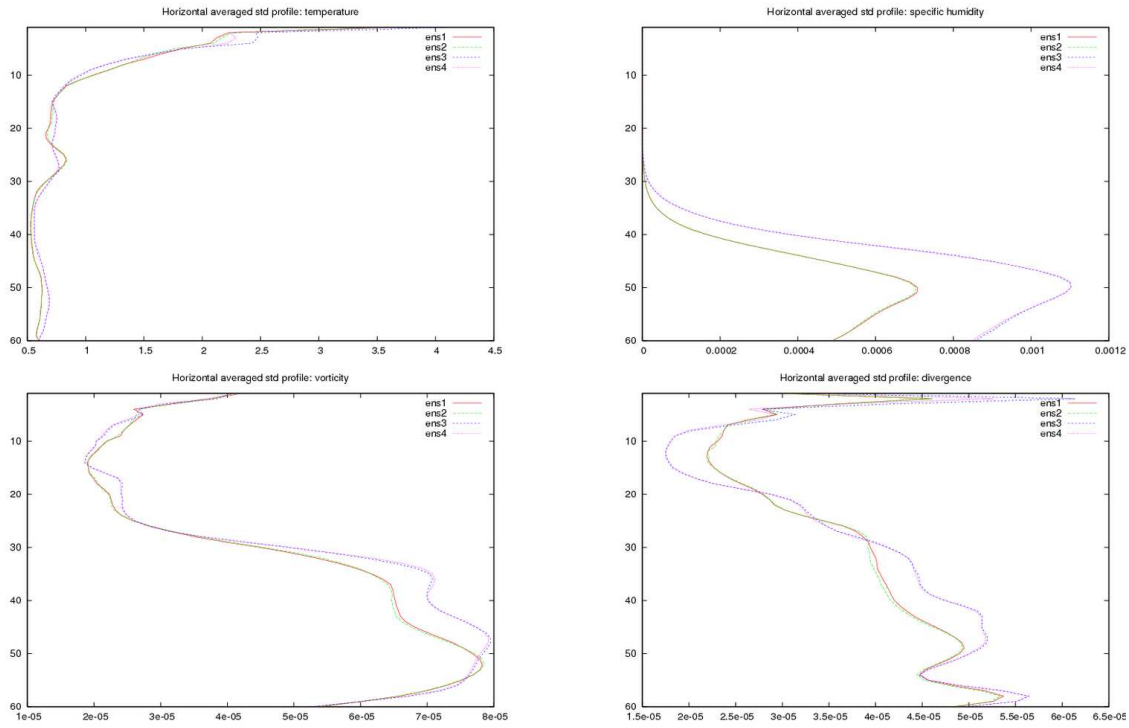

Figure 2: Horizontal averaged std values at 00UTC: temperature (top left; K), specific humidity (top right; kg kg-1), vorticity (bottom left; Jkg-1s) and divergence (bottom rigth; s-1); Y-axis: model levels

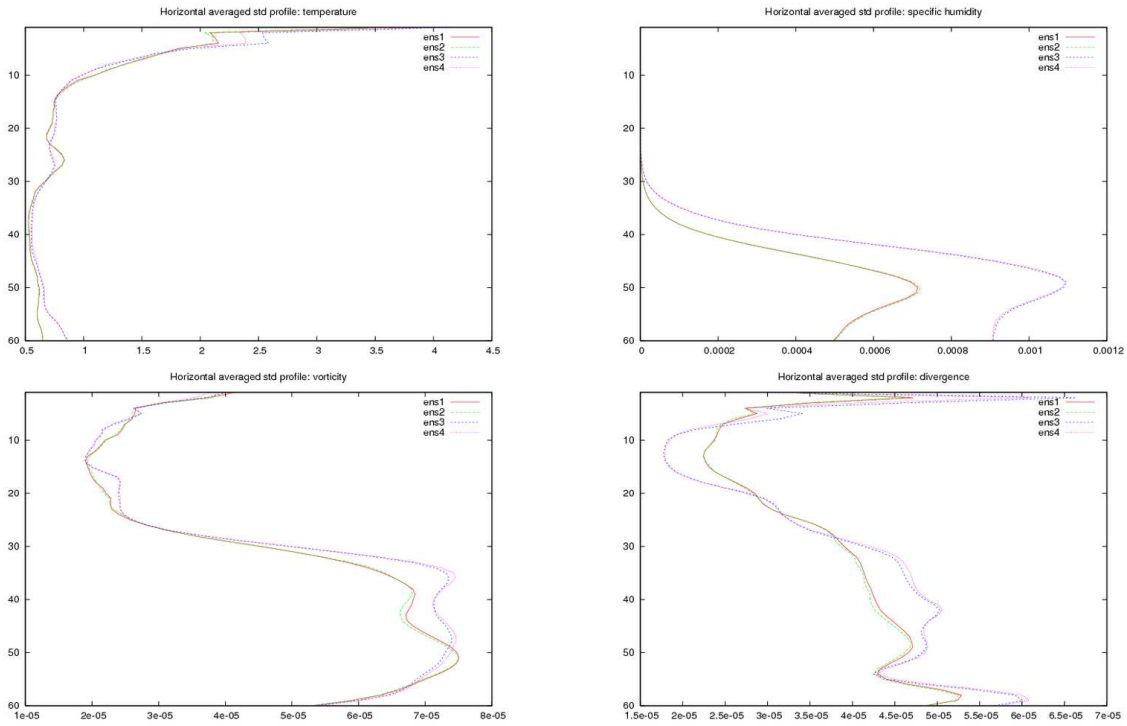

Figure 3: Horizontal averaged std values at 06UTC: temperature (top left; K), specific humidity (top right; kg kg-1), vorticity (bottom left; Jkg-1s) and divergence (bottom rigth; s-1); Y-axis: model levels

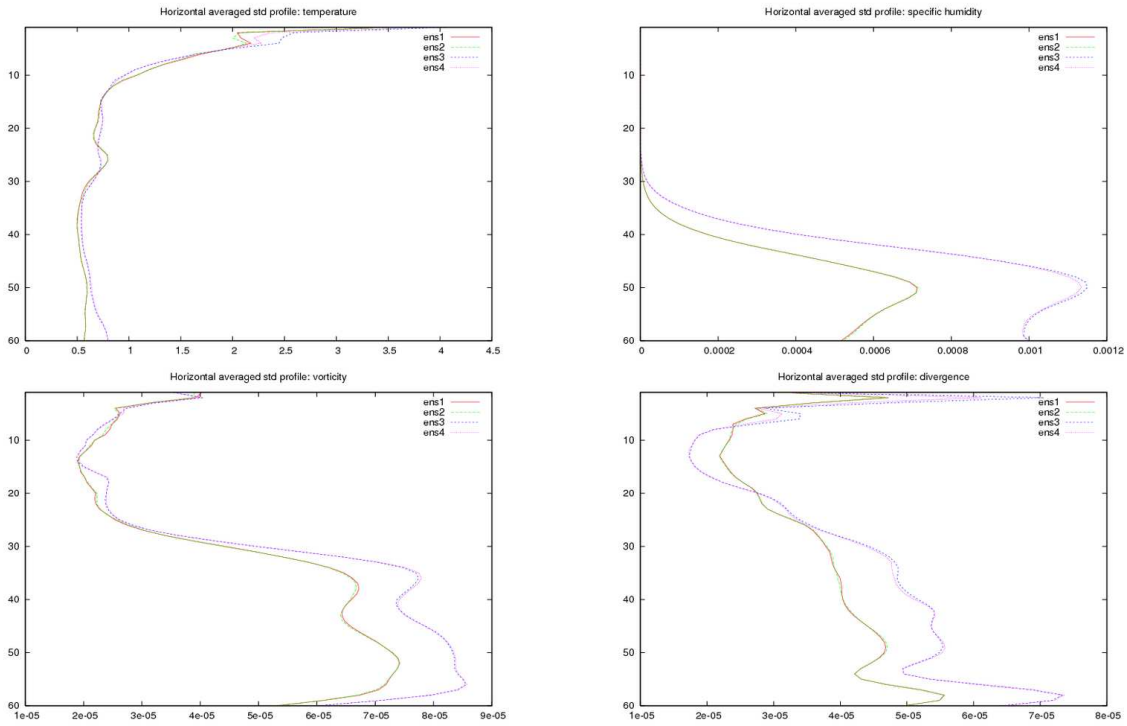

Figure 4: Horizontal averaged std values at 12UTC: temperature (top left; K), specific humidity (top right; kg kg-1), vorticity (bottom left; Jkg-1) and divergence (bottom rigth; s-1); Y-axis: model levels

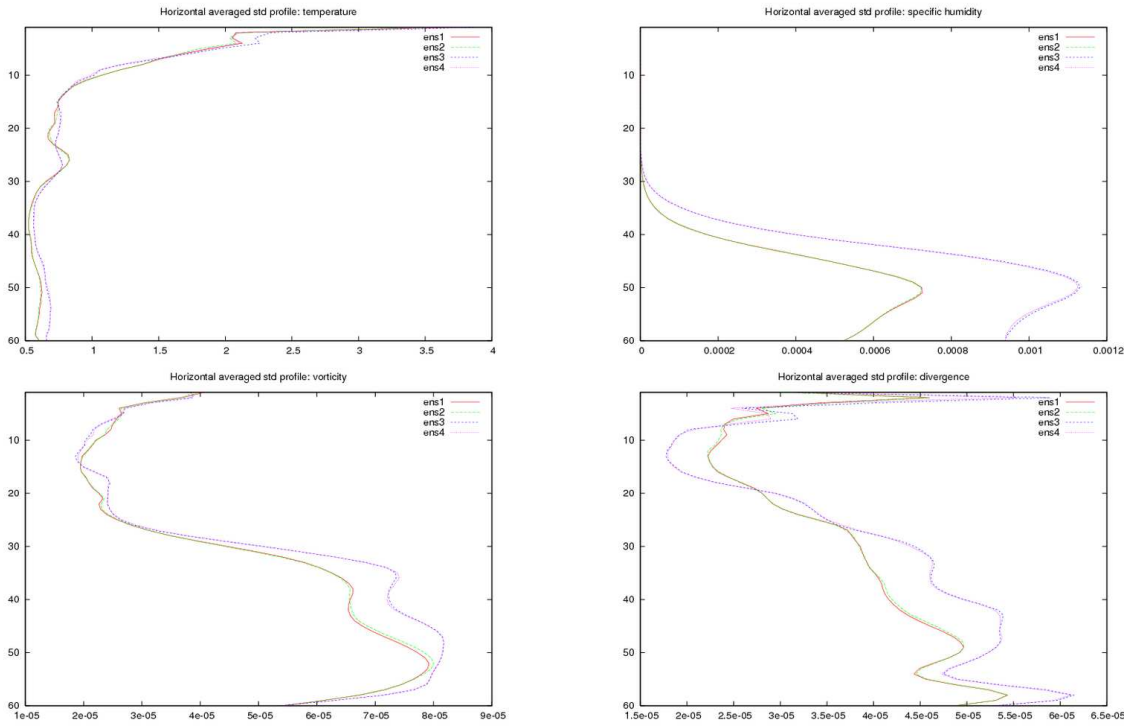

Figure 5: Horizontal averaged std values at 18UTC: temperature (top left; K), specific humidity (top right; kg kg-1), vorticity (bottom left; Jkg-1) and divergence (bottom rigth; s-1); Y-axis: model levels

A.2 Horizontal auto-correlations

A.2.1 Vertical profiles of horizontal length-scale - each network

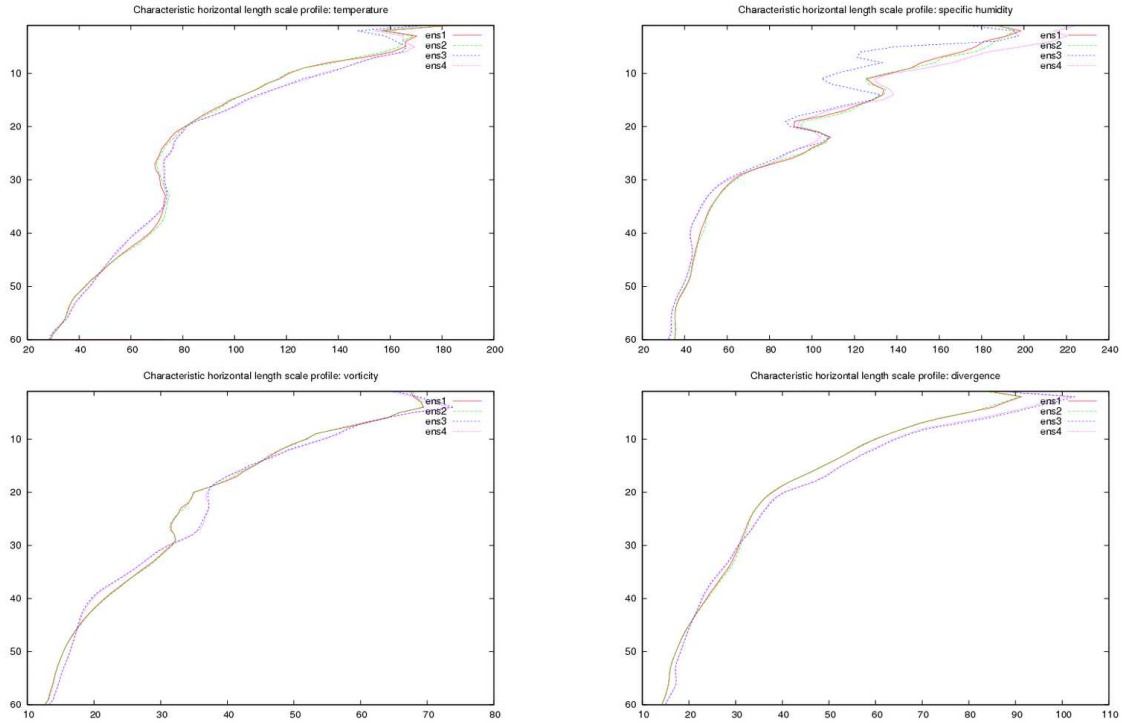

Figure 6: Horizontal averaged length-scale values at 00UTC: temperature (top left; K), specific humidity (top right; kg kg-1), vorticity (bottom left; Jkg-1 s) and divergence (bottom rigth; s-1); Y-axis: model levels

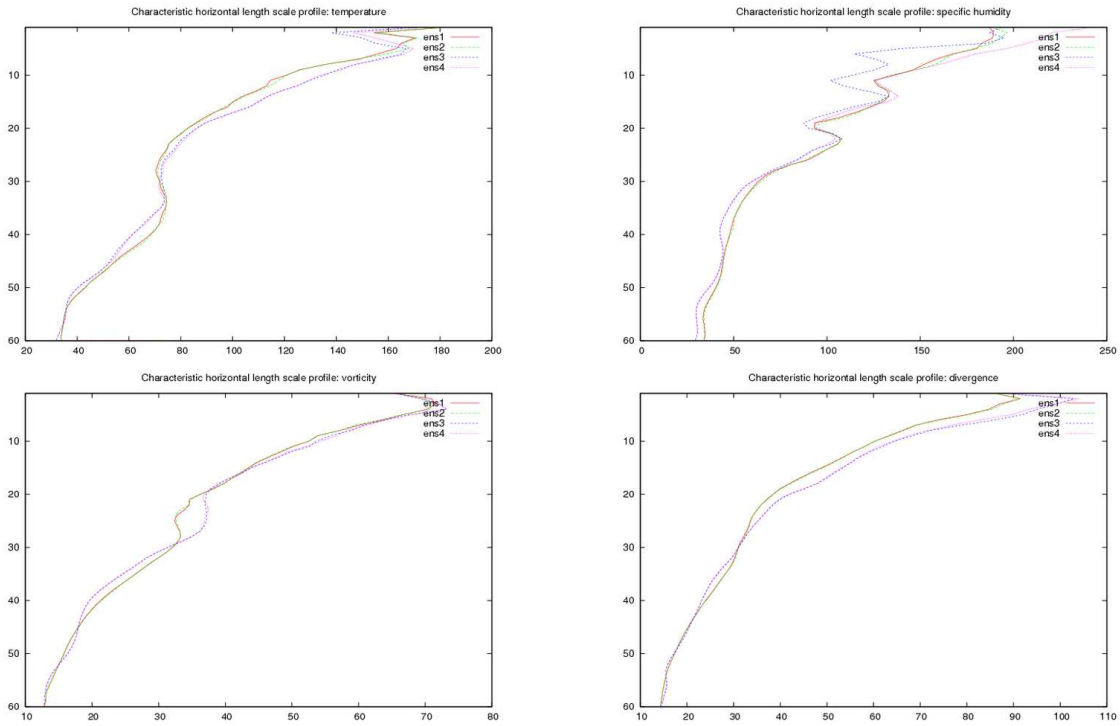

Figure 7: Horizontal averaged length-scale values at 06UTC: temperature (top left; K), specific humidity (top right; kg kg-1), vorticity (bottom left; Jkg-1 s) and divergence (bottom rigth; s-1); Y-axis: model levels

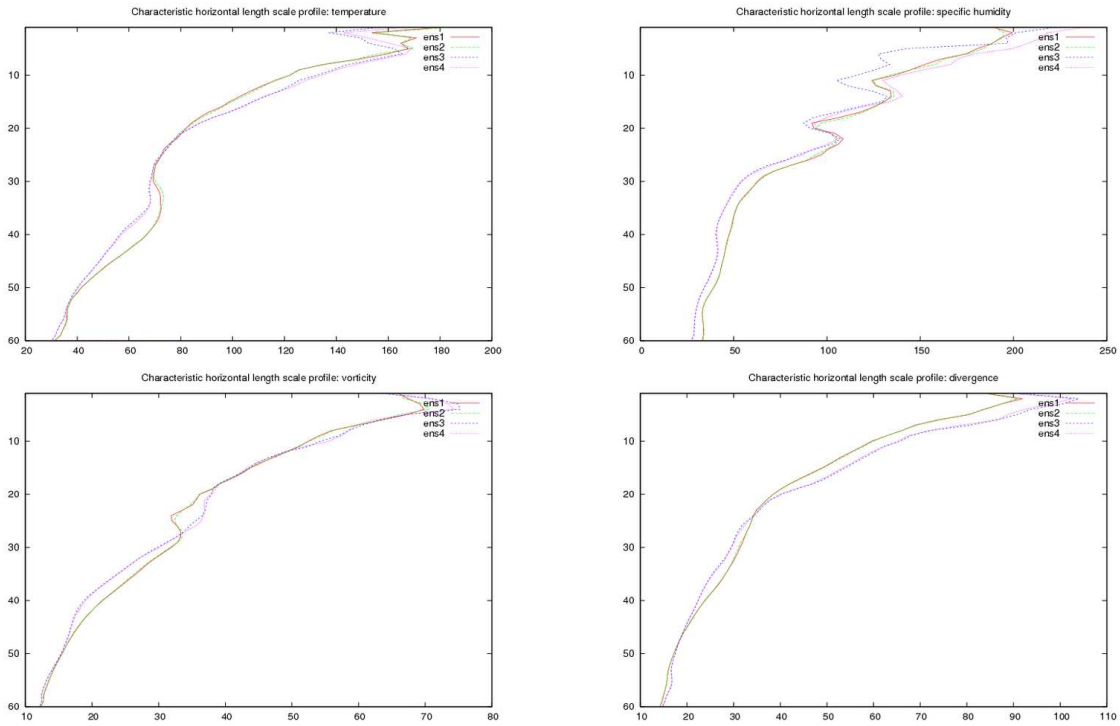

Figure 8: Horizontal averaged length-scale values at 12UTC: temperature (top left; K), specific humidity (top right; kg kg-1), vorticity (bottom left; Jkg-1 s) and divergence (bottom rigth; s-1); Y-axis: model levels

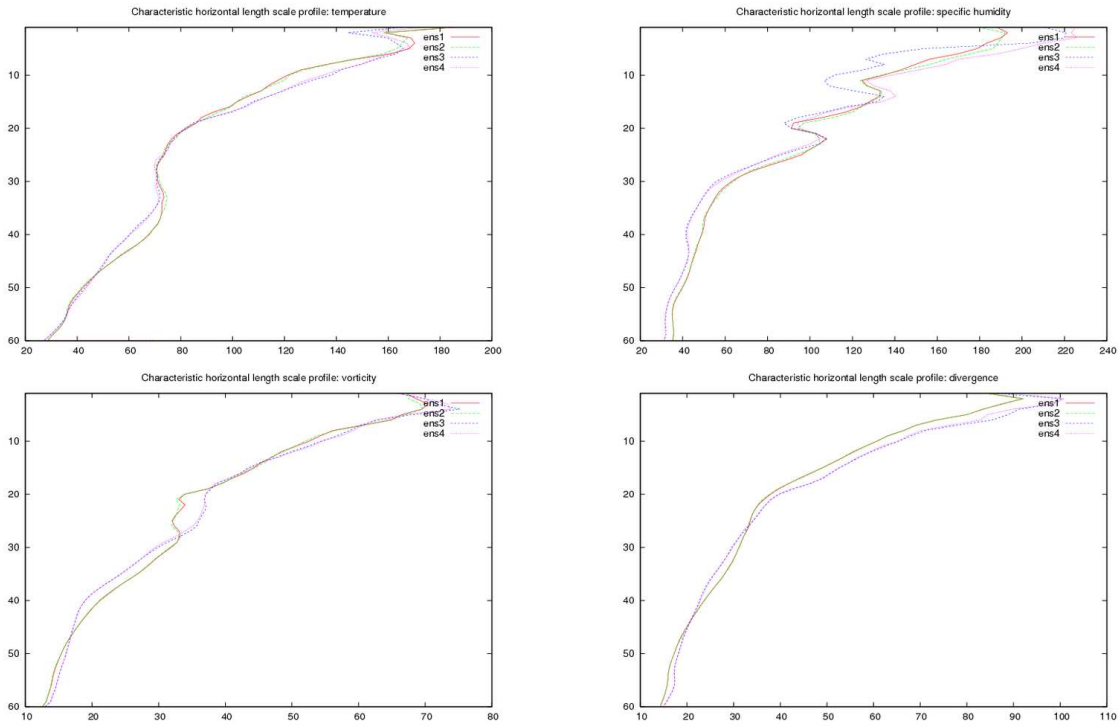

Figure 9: Horizontal averaged length-scale values at 18UTC: temperature (top left; K), specific humidity (top right; kg kg-1), vorticity (bottom left; Jkg-1 s) and divergence (bottom rigth; s-1); Y-axis: model levels

A.2.2 Variance spectra - each network

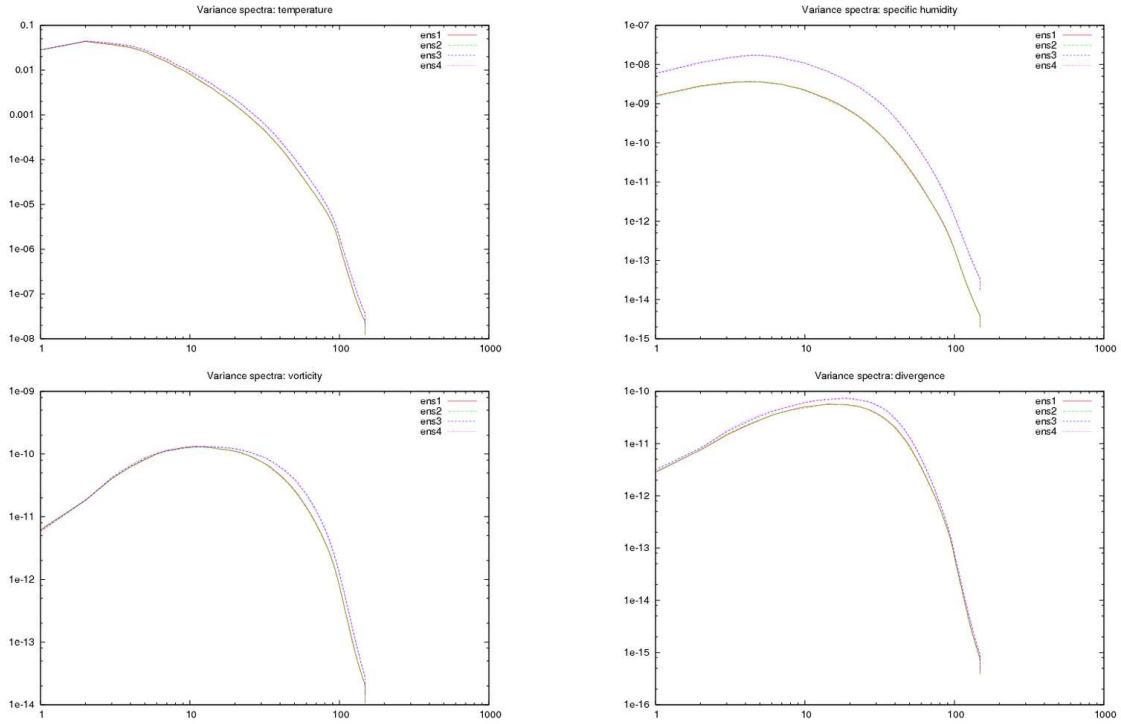

Figure 10: Averaged variance spectra values at 00UTC: temperature (top left; K), specific humidity (top right; kg kg-1), vorticity (bottom left; Jkg-1 s) and divergence (bottom rigth; s-1); X-axis: wave number

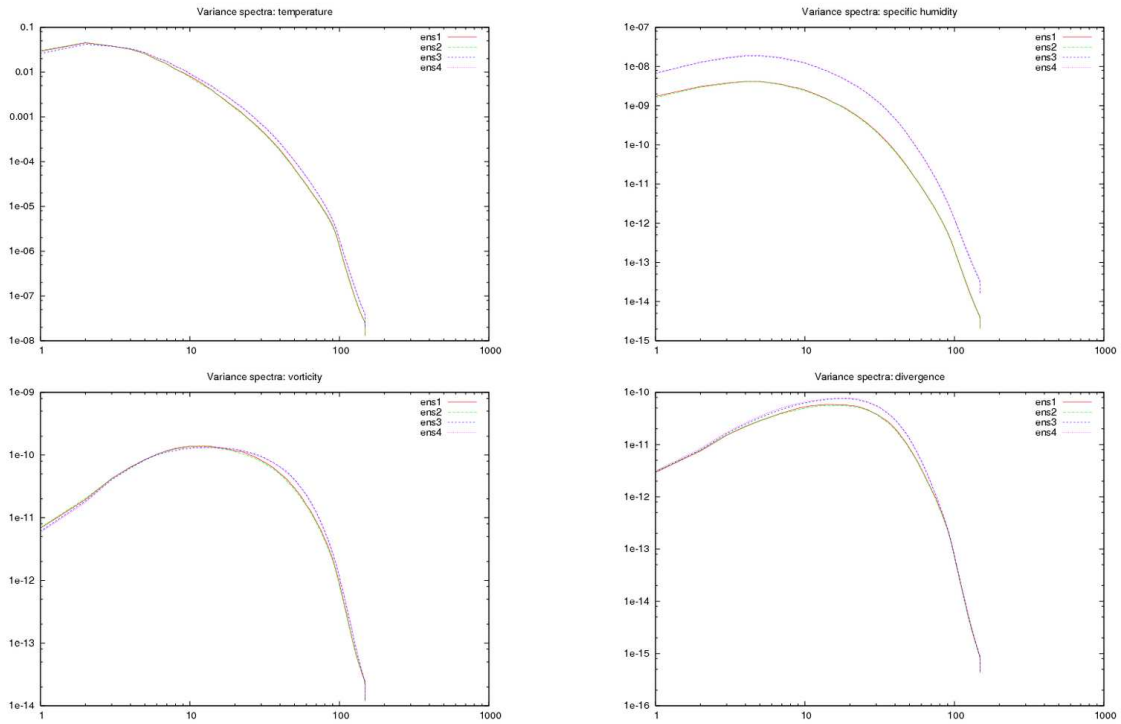

Figure 11: Averaged variance spectra values at 06UTC: temperature (top left; K), specific humidity (top right; kg kg-1), vorticity (bottom left; Jkg-1 s) and divergence (bottom rigth; s-1); X-axis: wave number

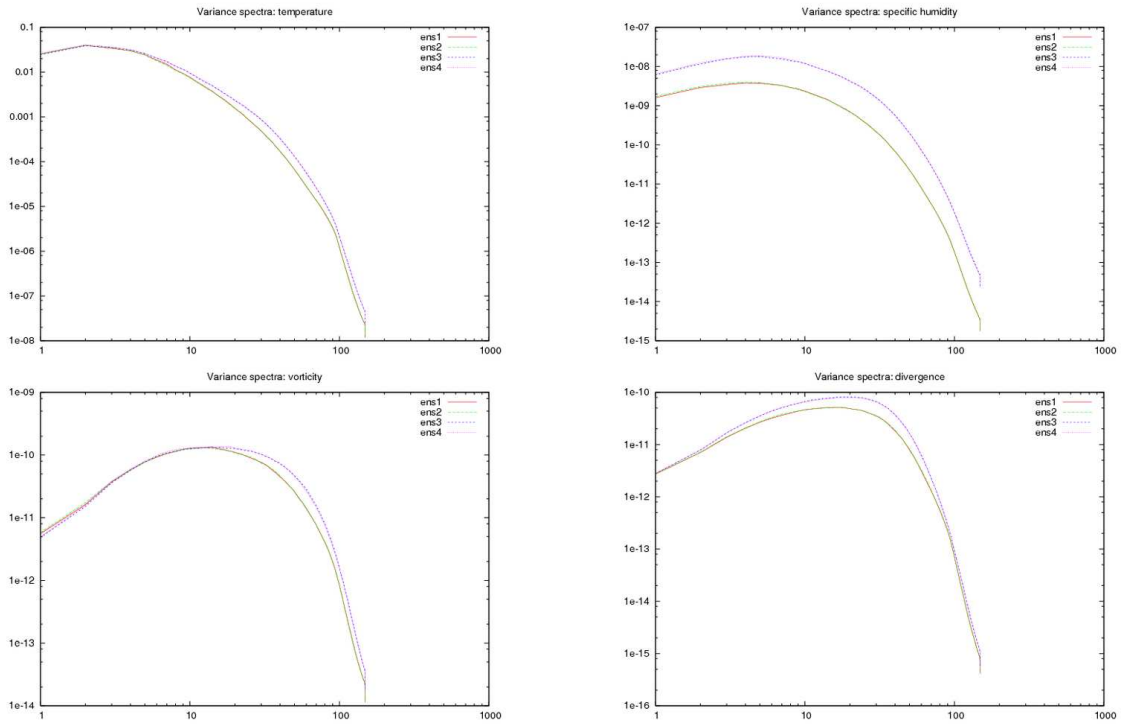

Figure 12: Averaged variance spectra values at 12UTC: temperature (top left; K), specific humidity (top right; kg kg-1), vorticity (bottom left; Jkg-1 s) and divergence (bottom rigth; s-1); X-axis: wave number

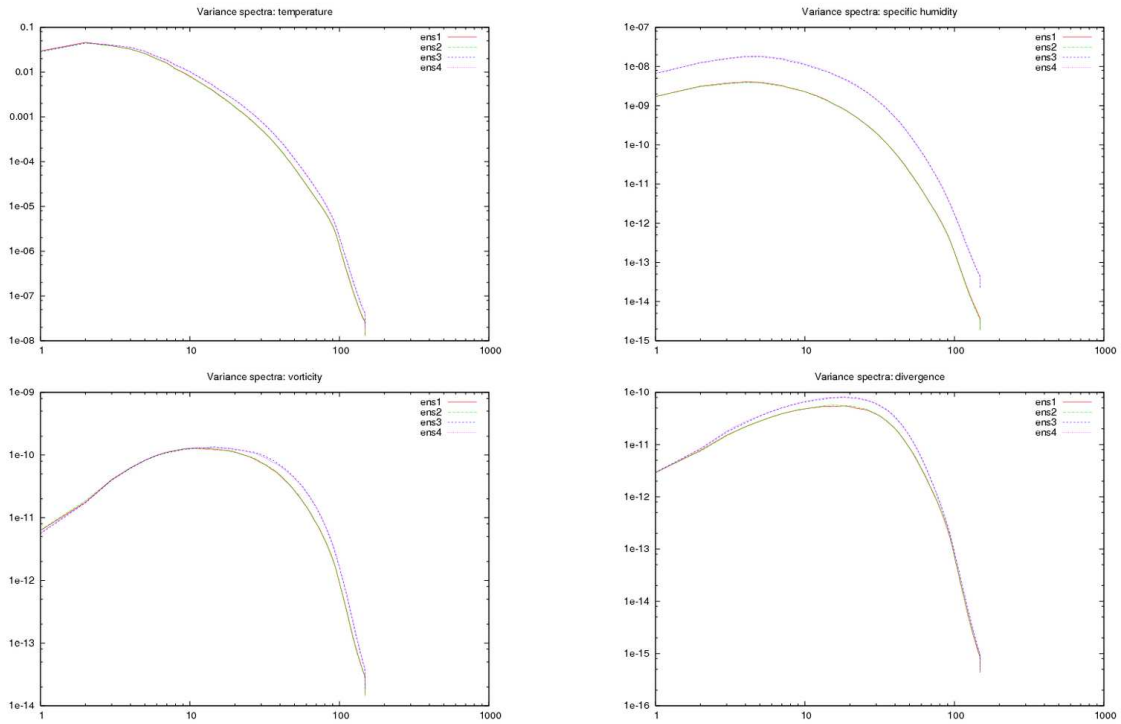

Figure 13: Averaged variance spectra values at 18UTC: temperature (top left; K), specific humidity (top right; kg kg-1), vorticity (bottom left; Jkg-1 s) and divergence (bottom rigth; s-1); X-axis: wave number

A.3 Vertical auto-correlations

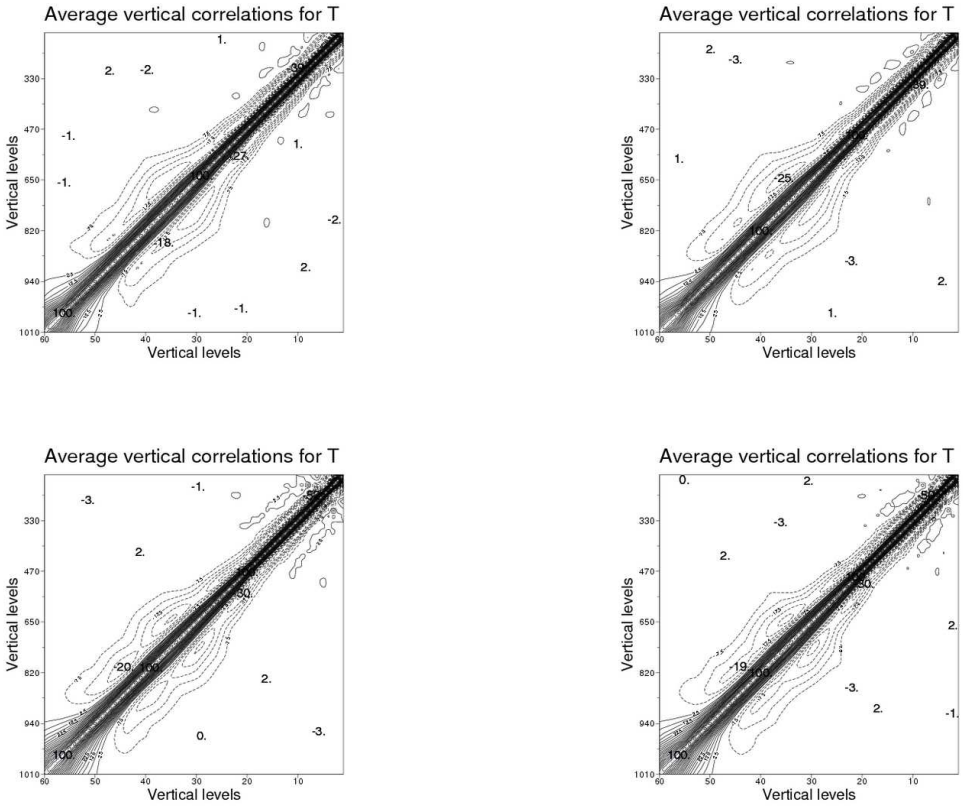

Figure 14: Vertical auto-correlations values for temperature at 00UTC: 1rst Winter ens (top left), 2nd Winter ens (top right), 1rst Summer ens (bottom left) and 2nd Summer ens (bottom rigth)

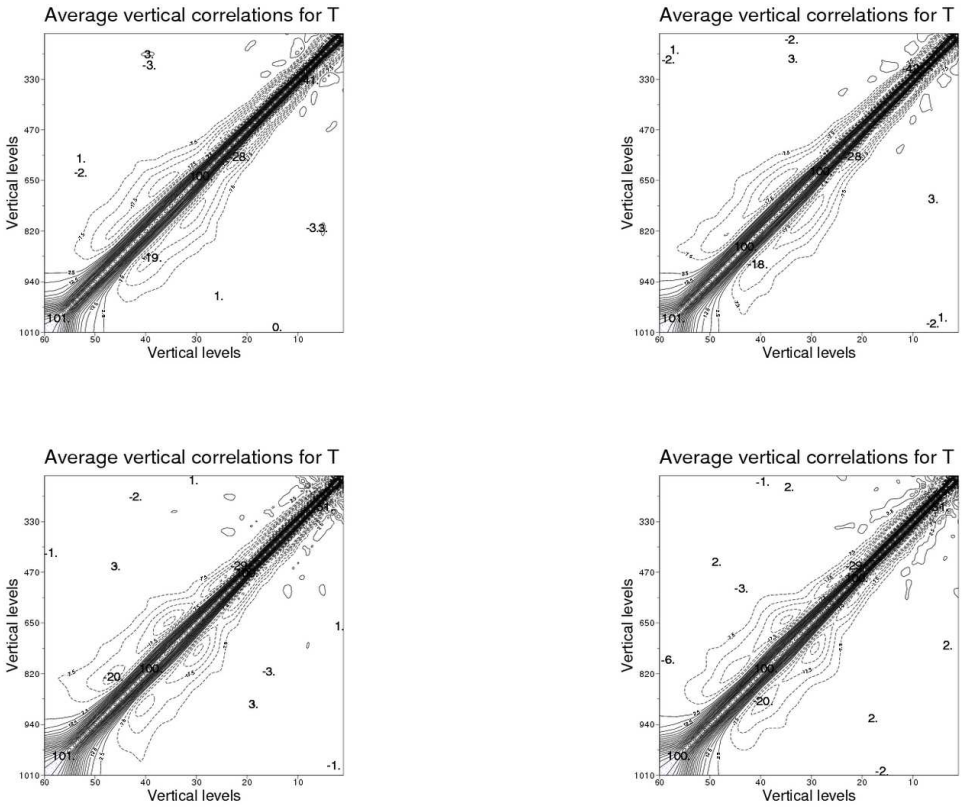

Figure 15: Vertical auto-correlations values for temperature at 06UTC: 1rst Winter ens (top left), 2nd Winter ens (top right), 1rst Summer ens (bottom left) and 2nd Summer ens (bottom rigth)

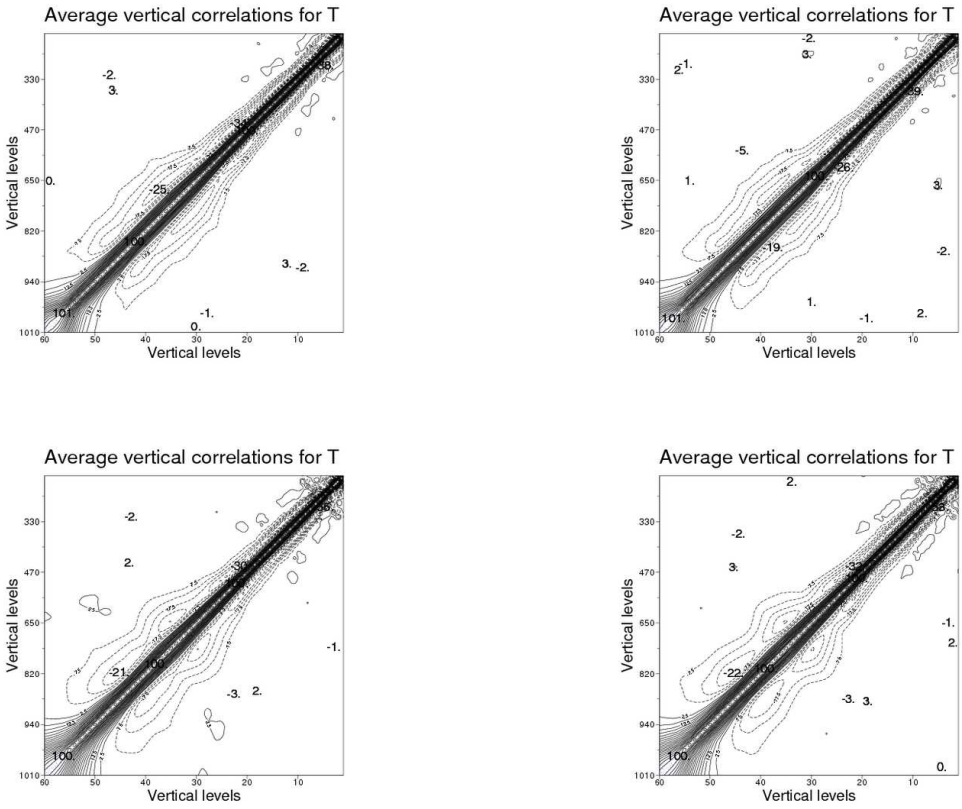

Figure 16: Vertical auto-correlations values for temperature at 12UTC: 1rst Winter ens (top left), 2nd Winter ens (top right), 1rst Summer ens (bottom left) and 2nd Summer ens (bottom rigth)

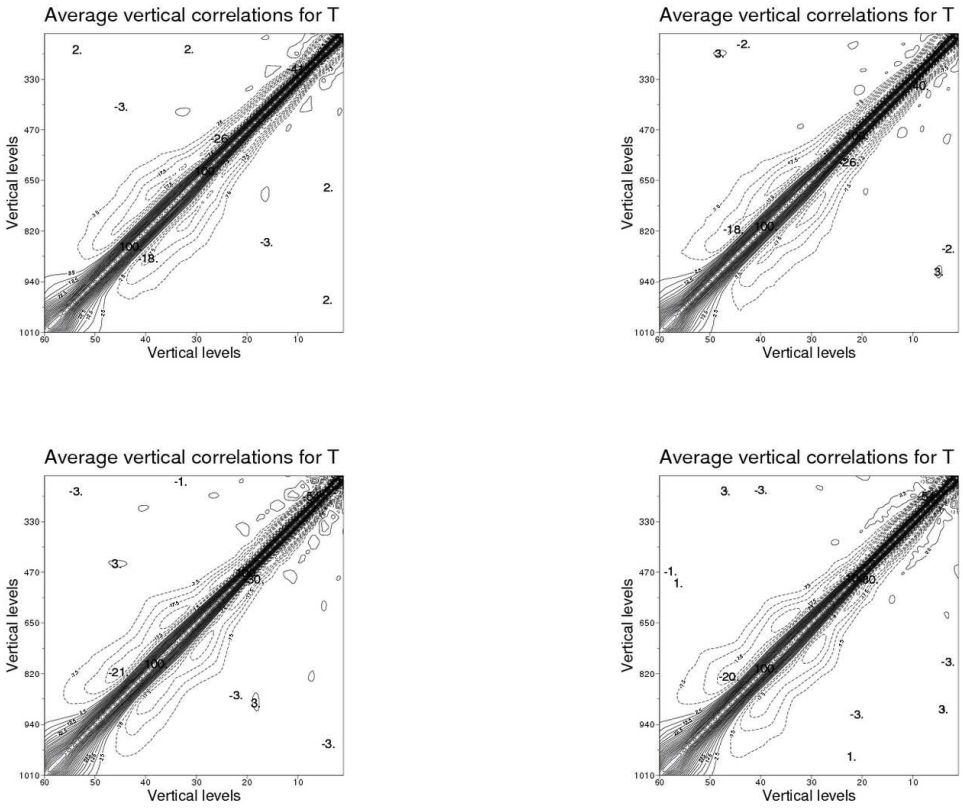

Figure 17: Vertical auto-correlations values for temperature at 18UTC: 1rst Winter ens (top left), 2nd Winter ens (top right), 1rst Summer ens (bottom left) and 2nd Summer ens (bottom rigth)

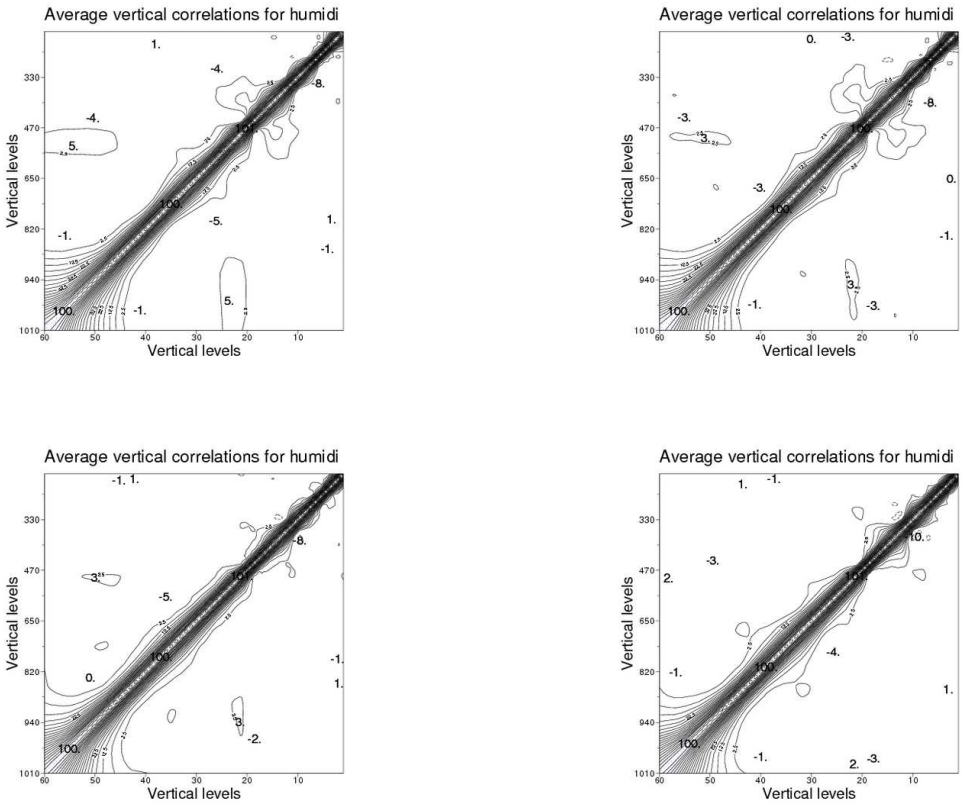

Figure 18: Vertical auto-correlation values for specific humidity at 00UTC: 1rst Winter ens (top left), 2nd Winter ens (top right), 1rst Summer ens (bottom left) and 2nd Summer ens (bottom rigth)

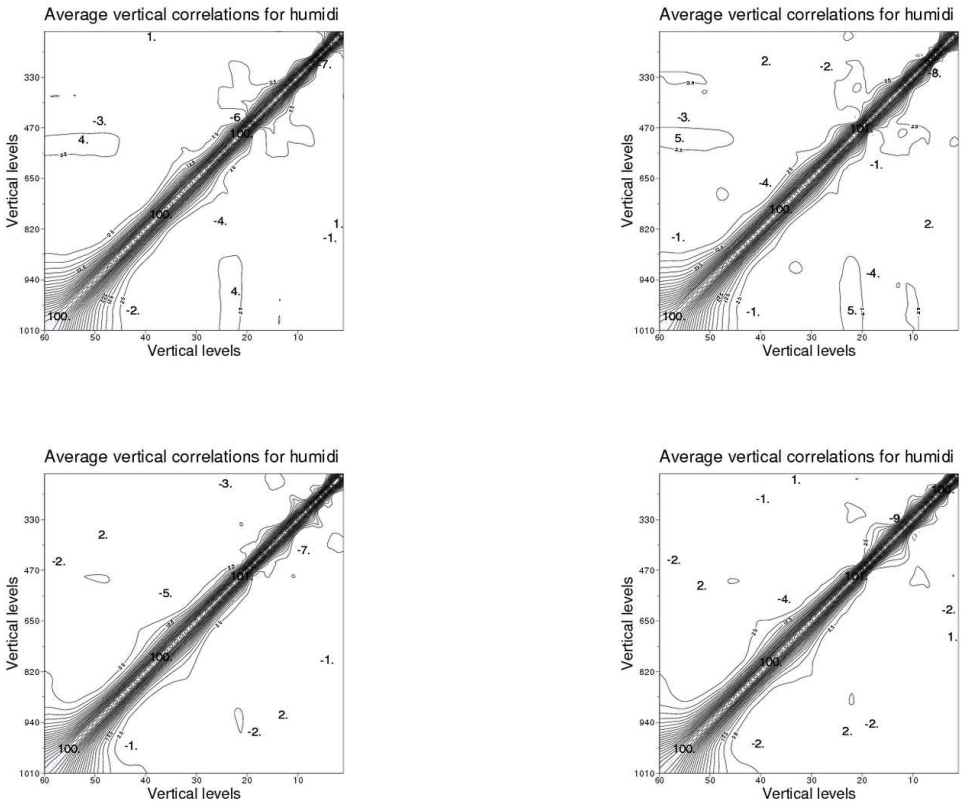

Figure 19: Vertical auto-correlation values for specific humidity at 06UTC: 1rst Winter ens (top left), 2nd Winter ens (top right), 1rst Summer ens (bottom left) and 2nd Summer ens (bottom rigth)

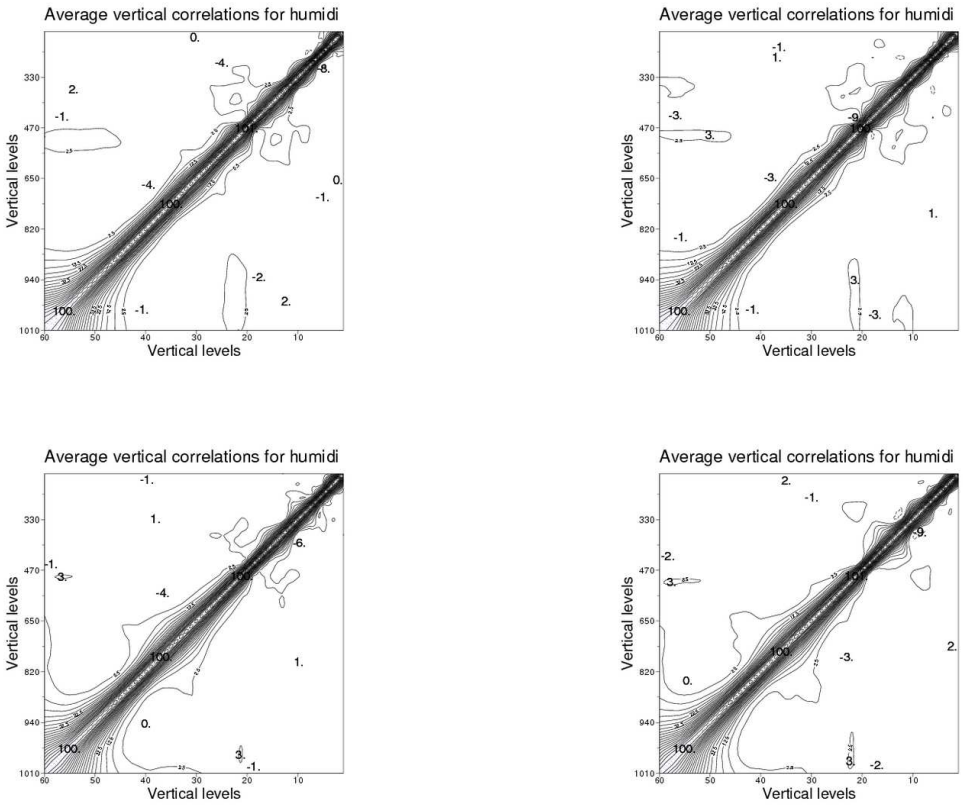

Figure 20: Vertical auto-correlation values for specific humidity at 12UTC: 1rst Winter ens (top left), 2nd Winter ens (top right), 1rst Summer ens (bottom left) and 2nd Summer ens (bottom rigth)

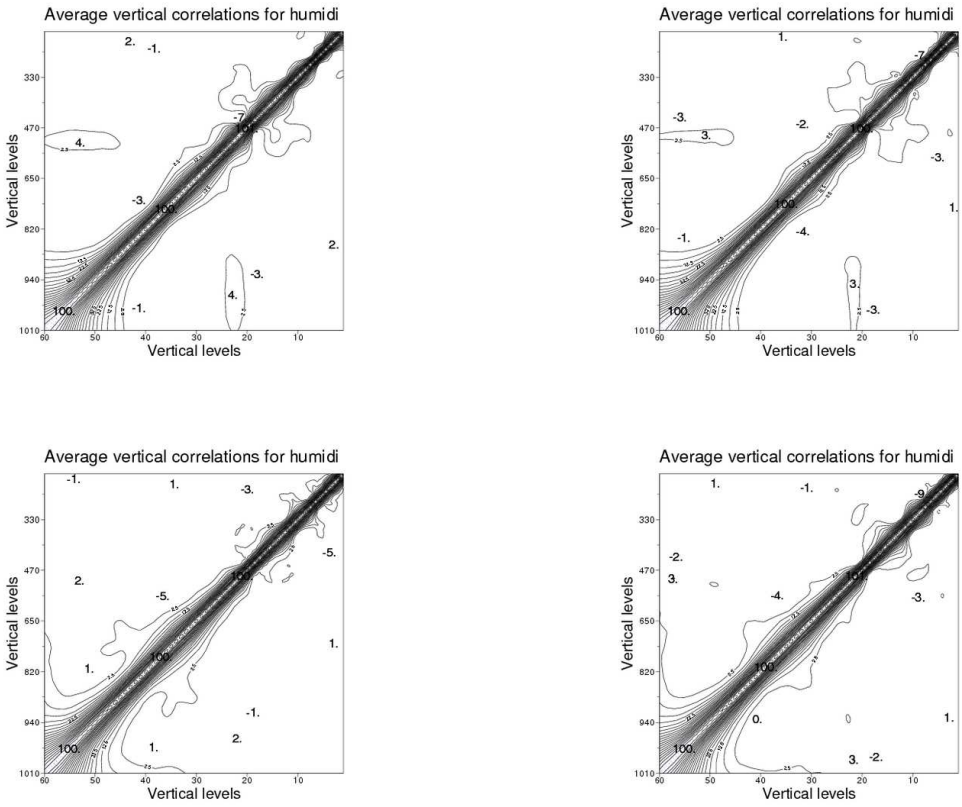

Figure 21: Vertical auto-correlation values for specific humidity at 18UTC: 1rst Winter ens (top left), 2nd Winter ens (top right), 1rst Summer ens (bottom left) and 2nd Summer ens (bottom rigth)

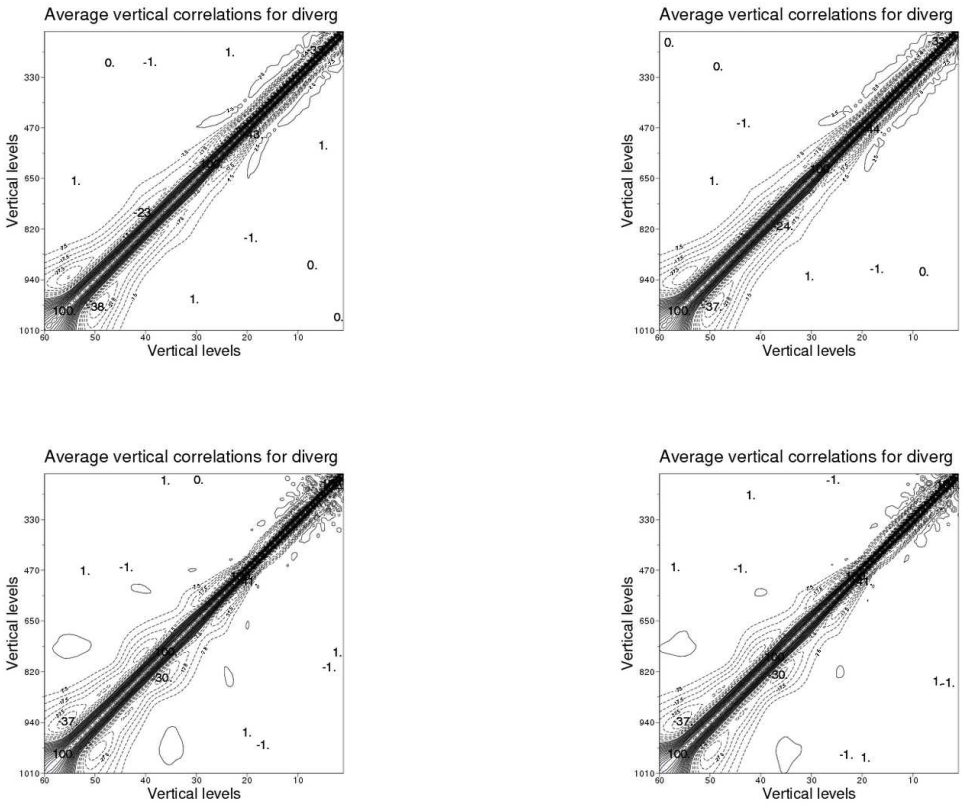

Figure 22: Vertical auto-correlation values for divergence at 00UTC: 1rst Winter ens (top left), 2nd Winter ens (top right), 1rst Summer ens (bottom left) and 2nd Summer ens (bottom rigth)

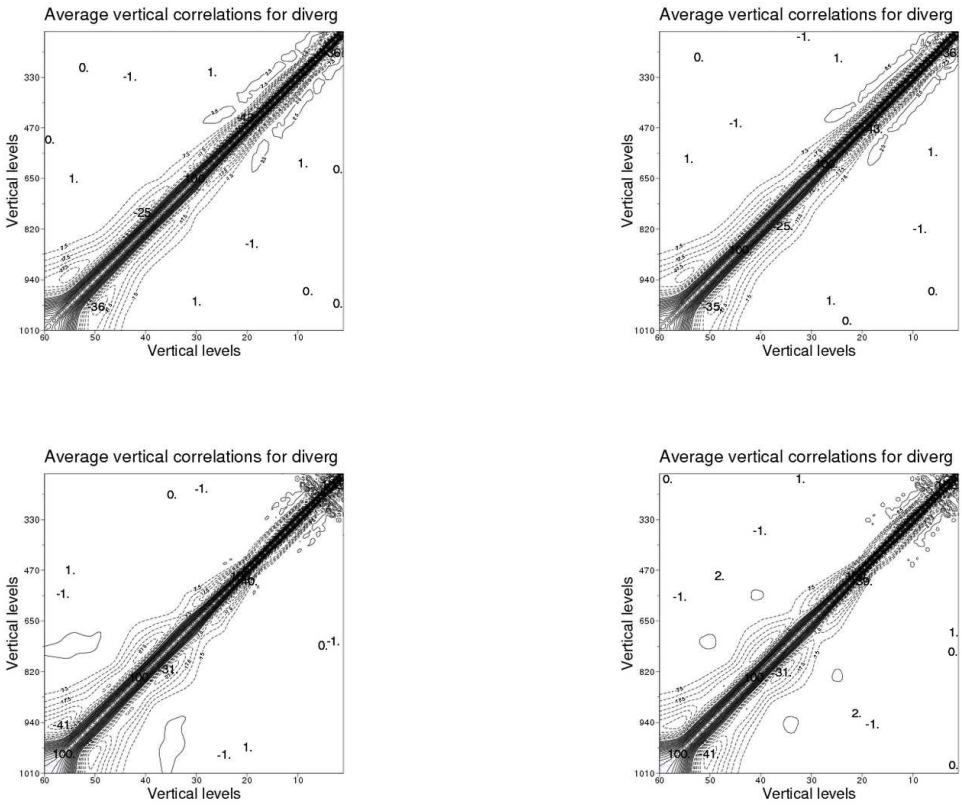

Figure 23: Vertical auto-correlation values for divergence at 06UTC: 1rst Winter ens (top left), 2nd Winter ens (top right), 1rst Summer ens (bottom left) and 2nd Summer ens (bottom rigth)

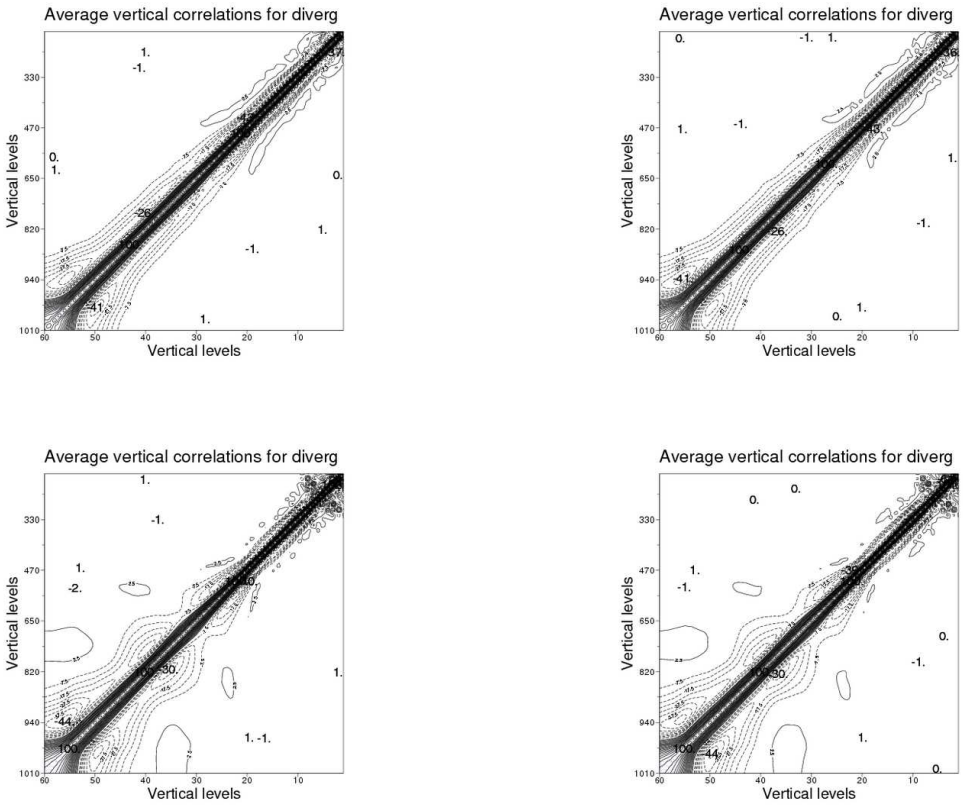

Figure 24: Vertical auto-correlation values for divergence at 12UTC: 1rst Winter ens (top left), 2nd Winter ens (top right), 1rst Summer ens (bottom left) and 2nd Summer ens (bottom rigth)

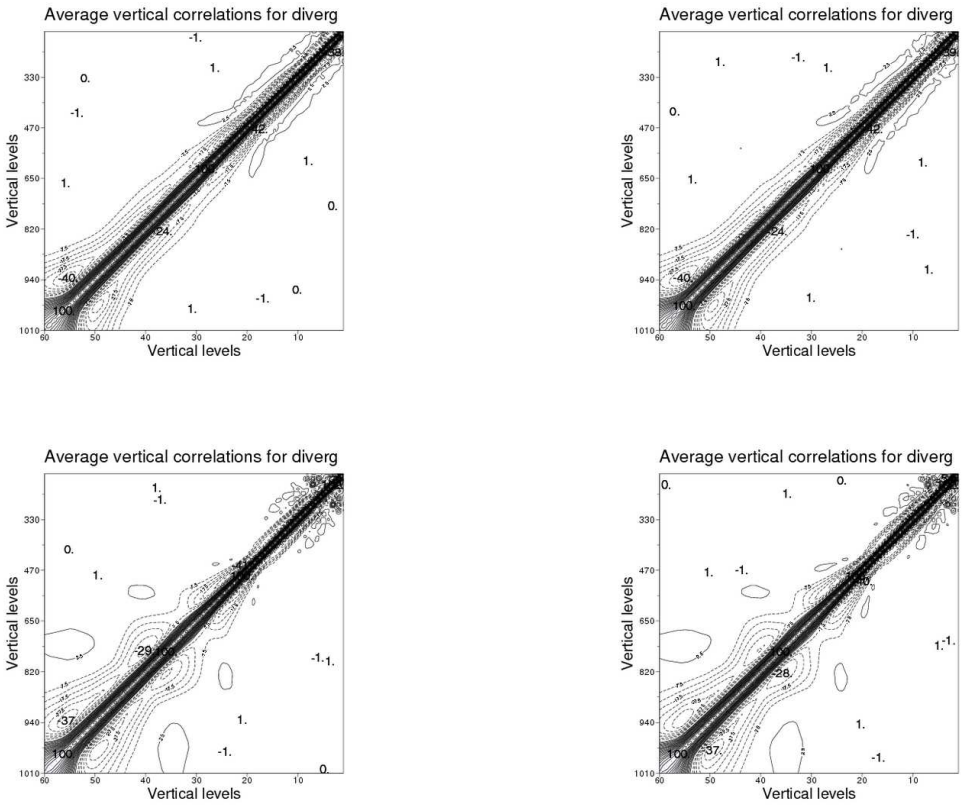

Figure 25: Vertical auto-correlation values for divergence at 18UTC: 1rst Winter ens (top left), 2nd Winter ens (top right), 1rst Summer ens (bottom left) and 2nd Summer ens (bottom rigth)

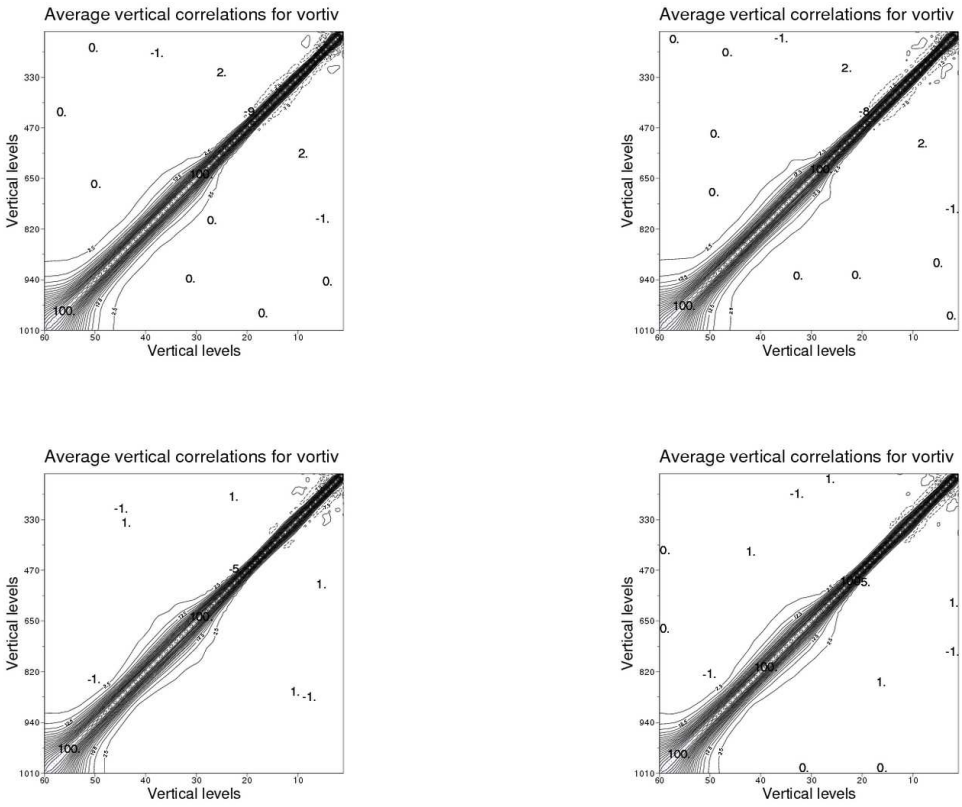

Figure 26: Vertical auto-correlation values for vorticity at 00UTC: 1rst Winter ens (top left), 2nd Winter ens (top right), 1rst Summer ens (bottom left) and 2nd Summer ens (bottom rigth)

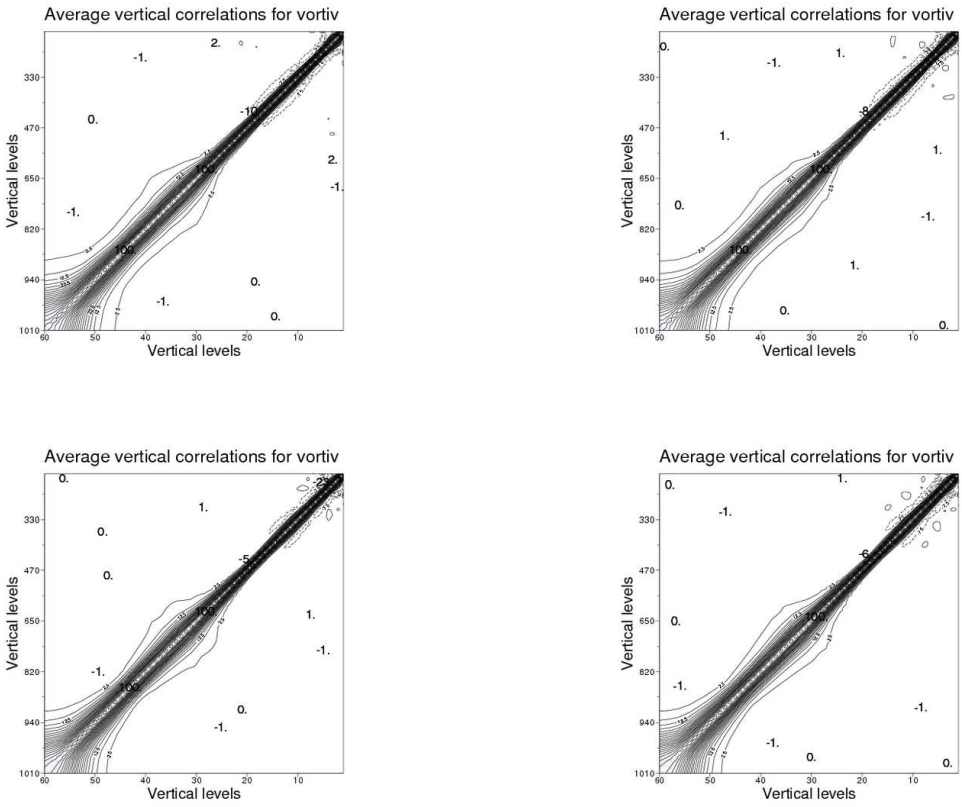

Figure 27: Vertical auto-correlation values for vorticity at 06UTC: 1rst Winter ens (top left), 2nd Winter ens (top right), 1rst Summer ens (bottom left) and 2nd Summer ens (bottom rigth)

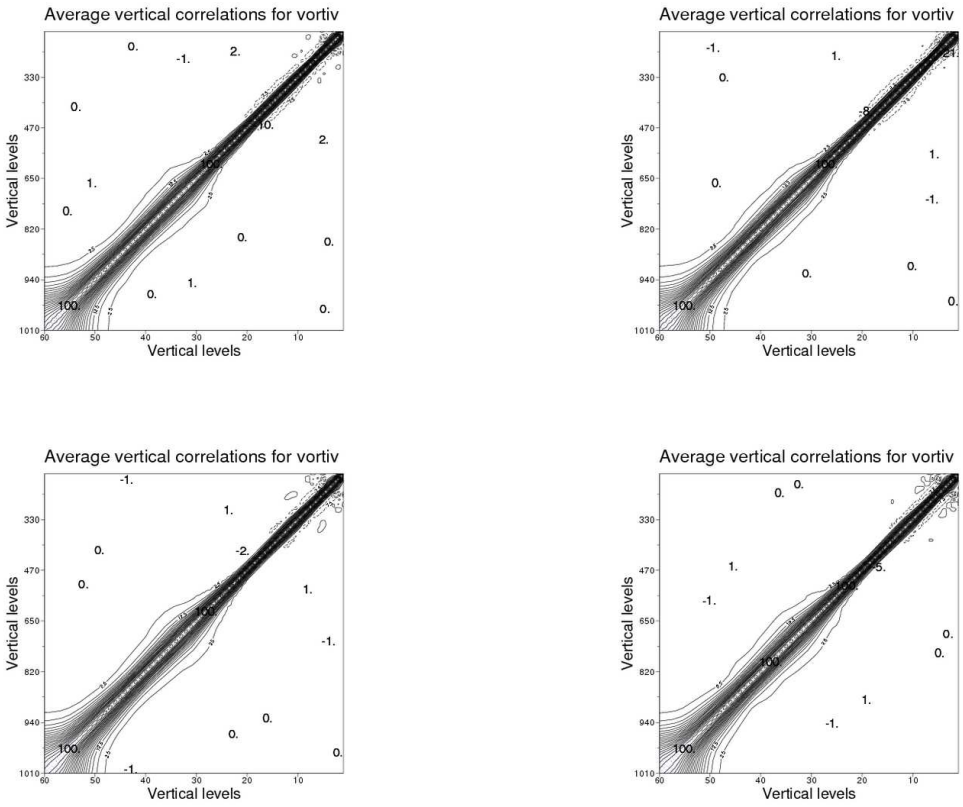

Figure 28: Vertical auto-correlation values for vorticity at 12UTC: 1rst Winter ens (top left), 2nd Winter ens (top right), 1rst Summer ens (bottom left) and 2nd Summer ens (bottom rigth)

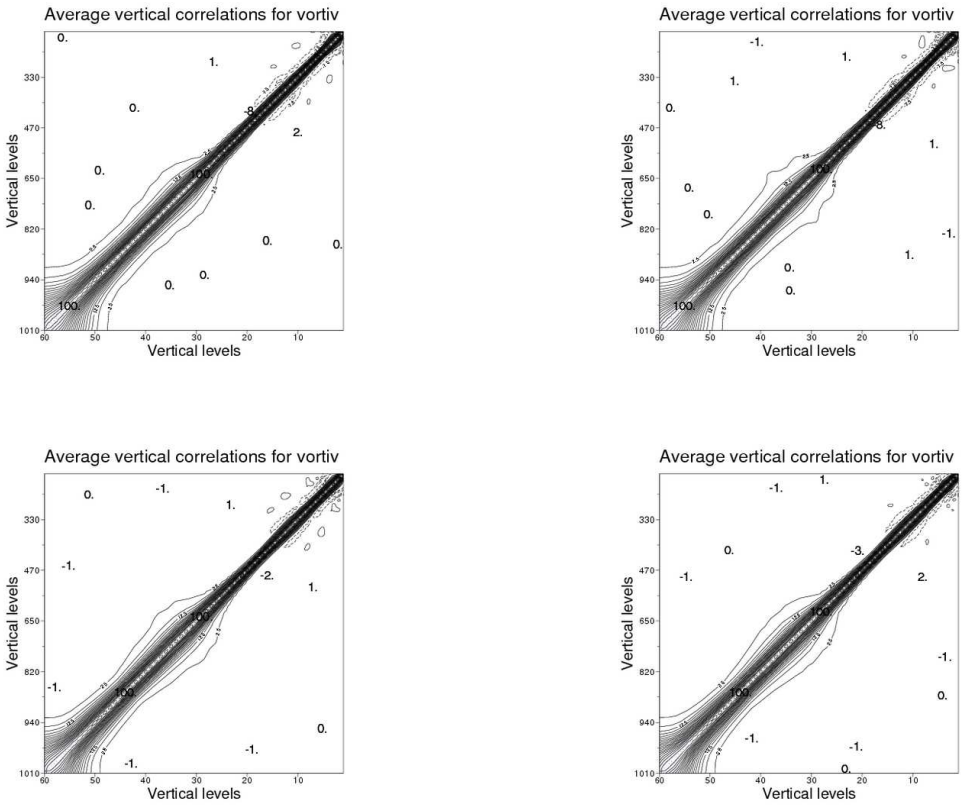

Figure 29: Vertical auto-correlation values for vorticity at 18UTC: 1rst Winter ens (top left), 2nd Winter ens (top right), 1rst Summer ens (bottom left) and 2nd Summer ens (bottom rigth)

A.4 Cross-covariances and percentages of explained variance

B Daily statistics

B.1 Total variance

B.1.1 Time evolution of averaged std at levels 850hPa and 500hPa - each network

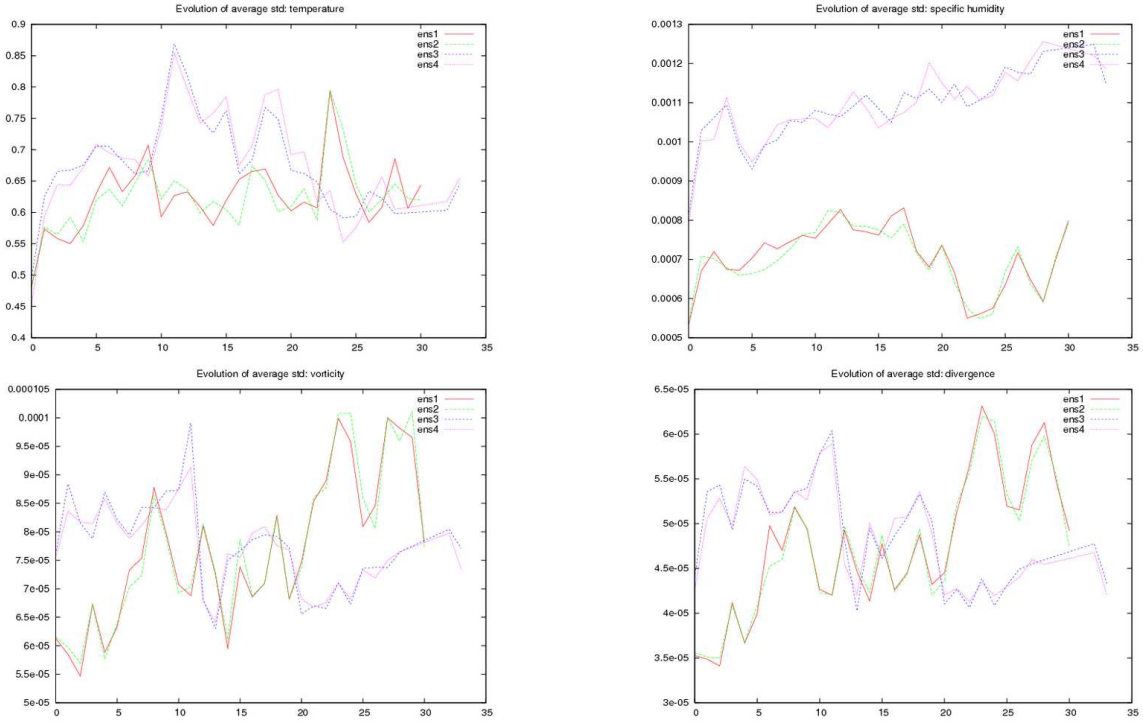

Figure 30: Time evolution of the averaged error background std for 850hPa at 00UTC: temperature (top left; K), specific humidity (top right; kg kg-1), vorticity (bottom left; Jkg-1 s) and divergence (bottom rigth; s-1); X-axis: number of run days

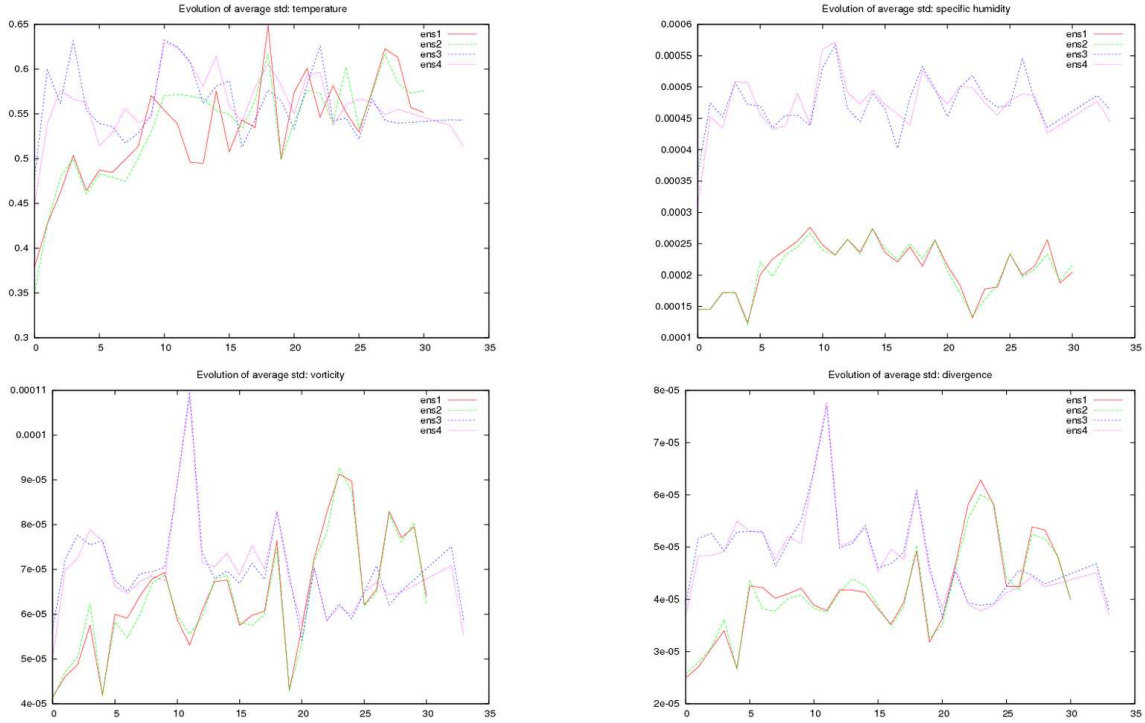

Figure 31: Time evolution of the averaged error background std for 500hPa at 00UTC: temperature (top left; K), specific humidity (top right; kg kg-1), vorticity (bottom left; Jkg-1 s) and divergence (bottom rigth; s-1); X-axis: number of run days

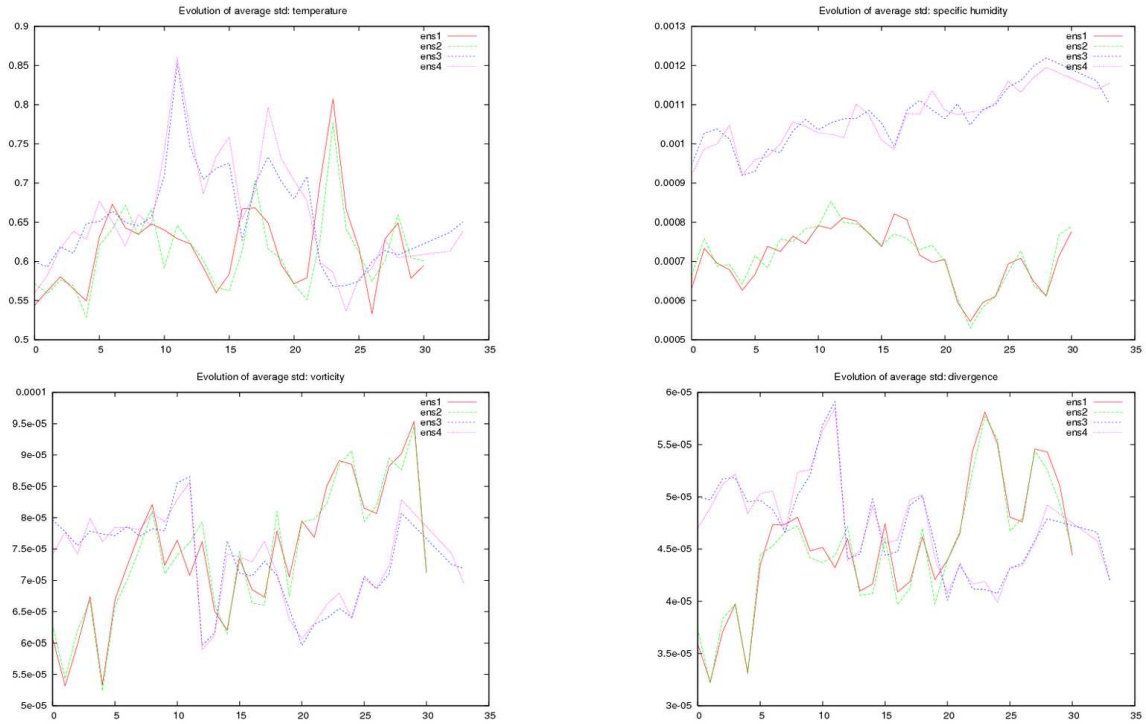

Figure 32: Time evolution of the averaged error background std for 850hPa at 06UTC: temperature (top left; K), specific humidity (top right; kg kg-1), vorticity (bottom left; Jkg-1 s) and divergence (bottom rigth; s-1); X-axis: number of run days)

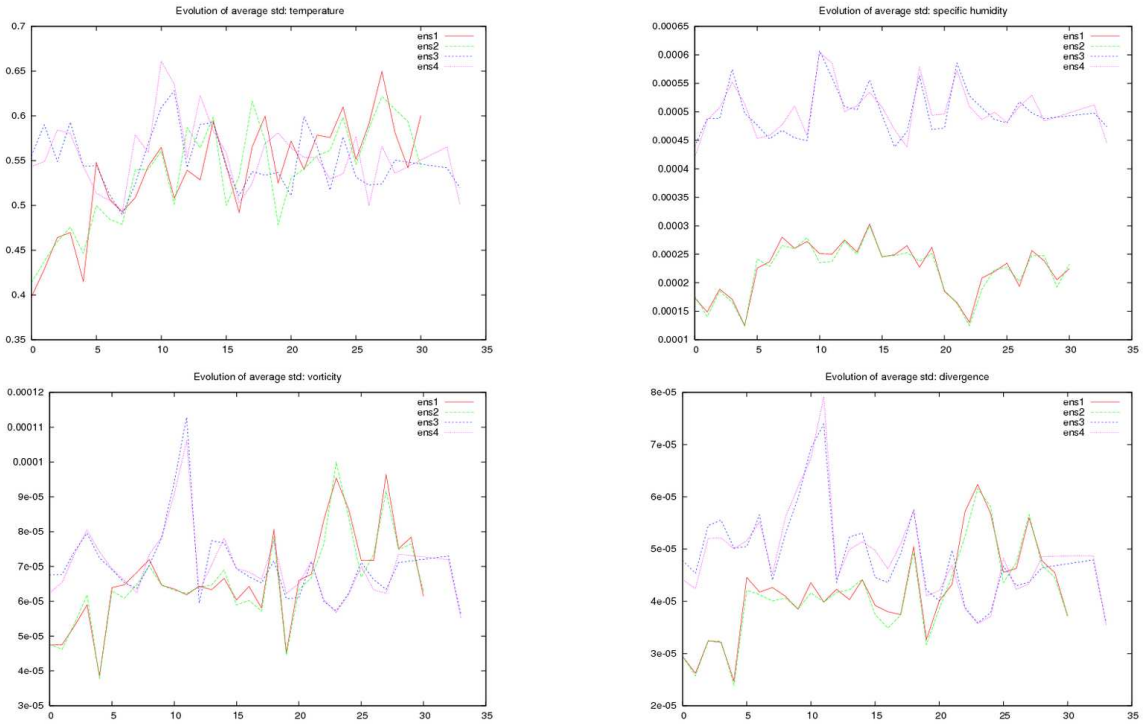

Figure 33: Time evolution of the averaged error background std for 500hPa at 06UTC: temperature (top left), specific humidity (top right), vorticity (bottom left; Jkg-1 s) and divergence (bottom rigth; s-1); X-axis: number of run days)

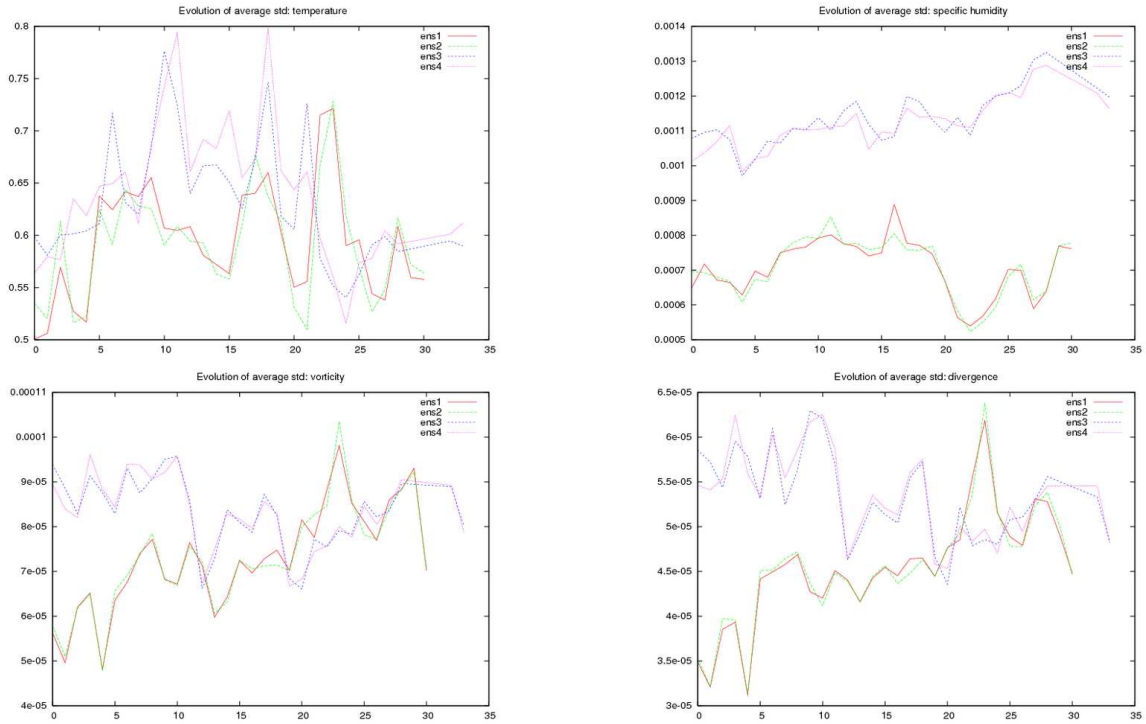

Figure 34: Time evolution of the averaged error background for 500hPa at 12UTC: temperature (top left; K), specific humidity (top right; kg kg-1), vorticity (bottom left; Jkg-1 s) and divergence (bottom rigth; s-1); X-axis: number of run days)

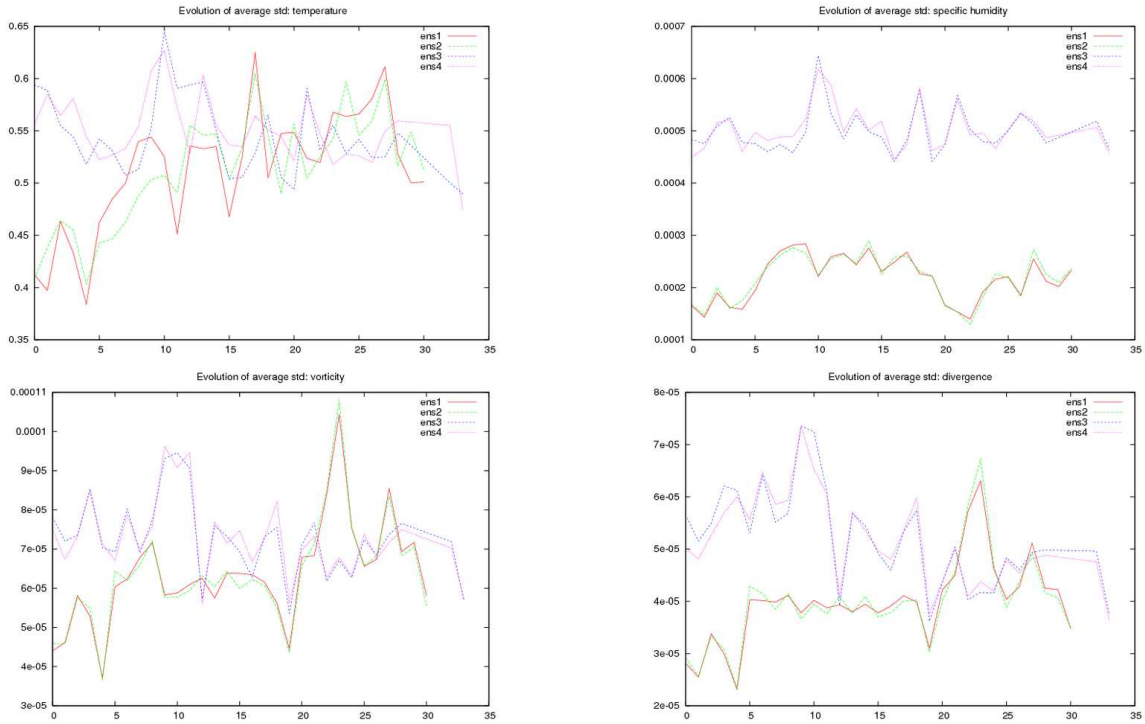

Figure 35: Time evolution of the averaged error background for 850hPa at 12UTC: temperature (top left; K), specific humidity (top right; kg kg-1), vorticity (bottom left; Jkg-1 s) and divergence (bottom rigth; s-1); X-axis: number of run days)

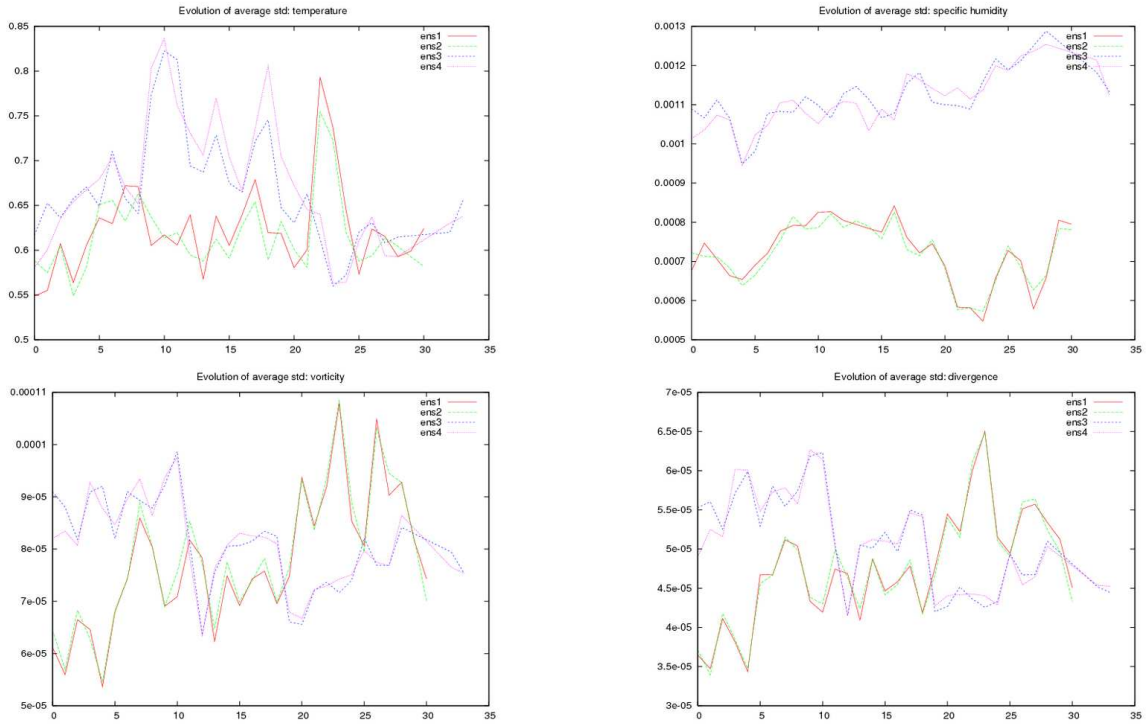

Figure 36: Time evolution of the averaged error background std for 850hPa at 18UTC: temperature (top left; K), specific humidity (top right; kg kg-1), vorticity (bottom left; Jkg-1 s) and divergence (bottom rigth; s-1); X-axis: number of run days)

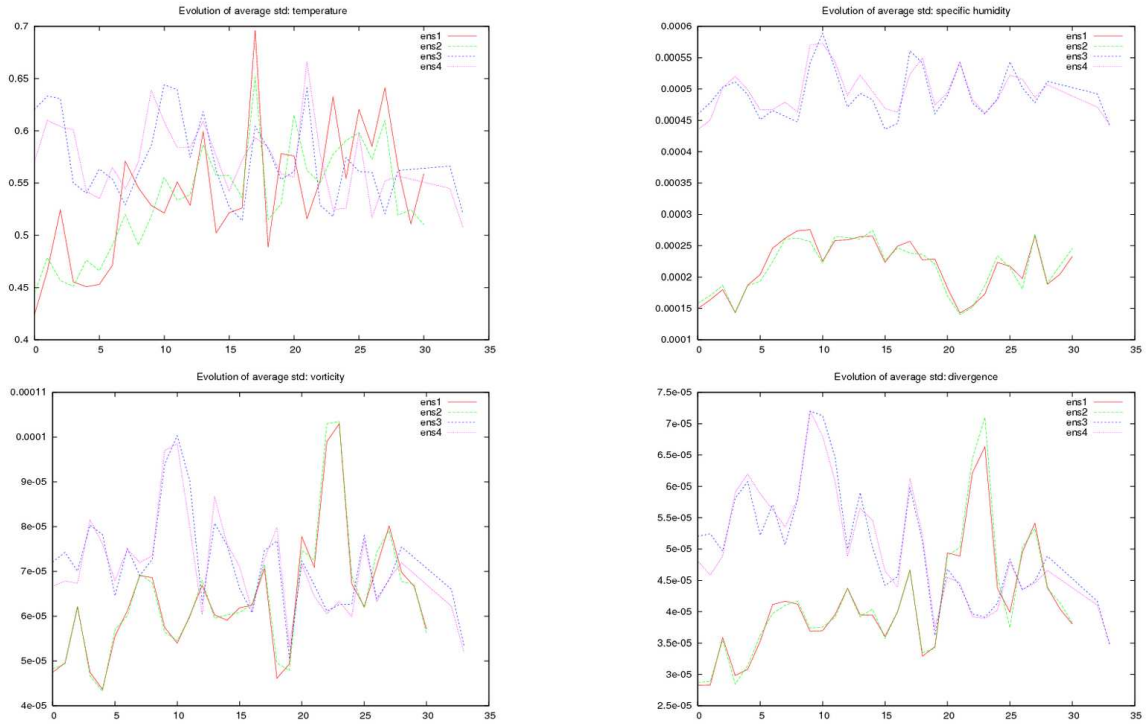

Figure 37: Time evolution of the averaged error background std for 500hPa at 18UTC: temperature (top left; K), specific humidity (top right; kg kg-1), vorticity (bottom left; Jkg-1 s) and divergence (bottom rigth; s-1); X-axis: number of run days)

B.2 Horizontal auto-correlations

B.2.1 Time evolution of horizontal length-scale at levels 850hPa and 500hPa - all networks

B.2.2 Time evolution of horizontal length-scale at levels 850hPa and 500hPa - each network

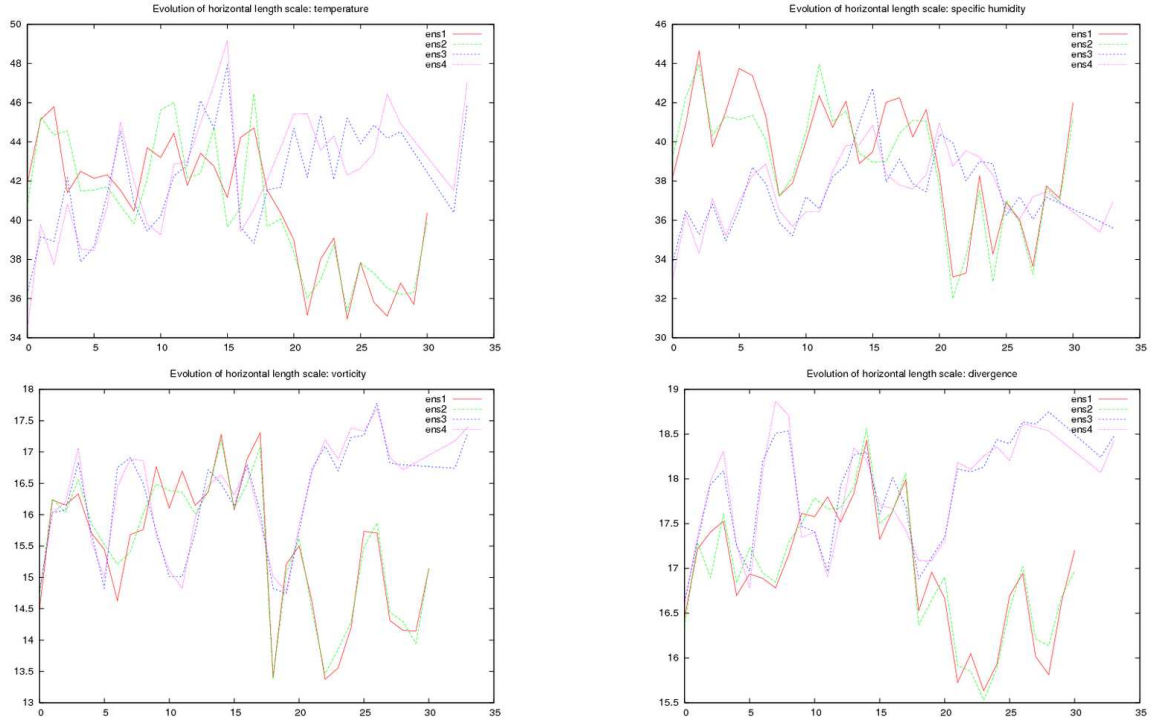

Figure 38: Time evolution of horizontal length-scale for 850hPa at 00UTC: temperature (top left; K), specific humidity (top right; kg kg-1), vorticity (bottom left; Jkg-1 s) and divergence (bottom rigth; s-1); X-axis: number of run days)

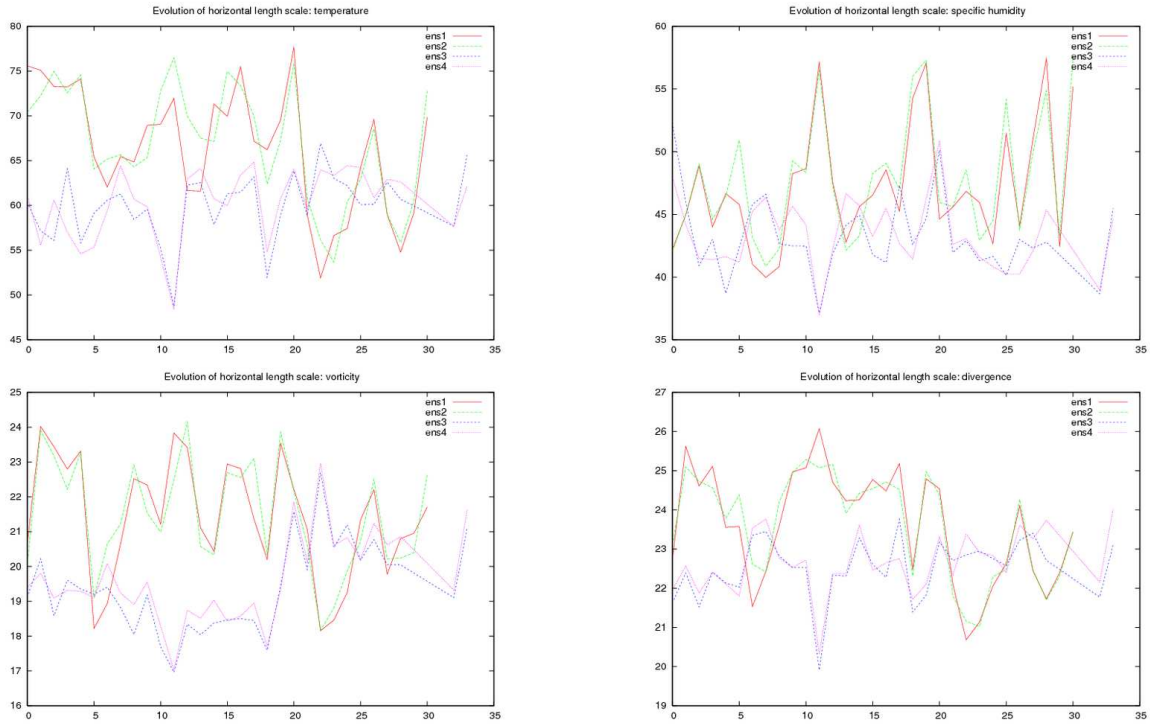

Figure 39: Time evolution of horizontal length-scale for 500hPa at 00UTC: temperature (top left; K), specific humidity (top right; kg kg-1), vorticity (bottom left; Jkg-1 s) and divergence (bottom rigth; s-1); X-axis: number of run days)

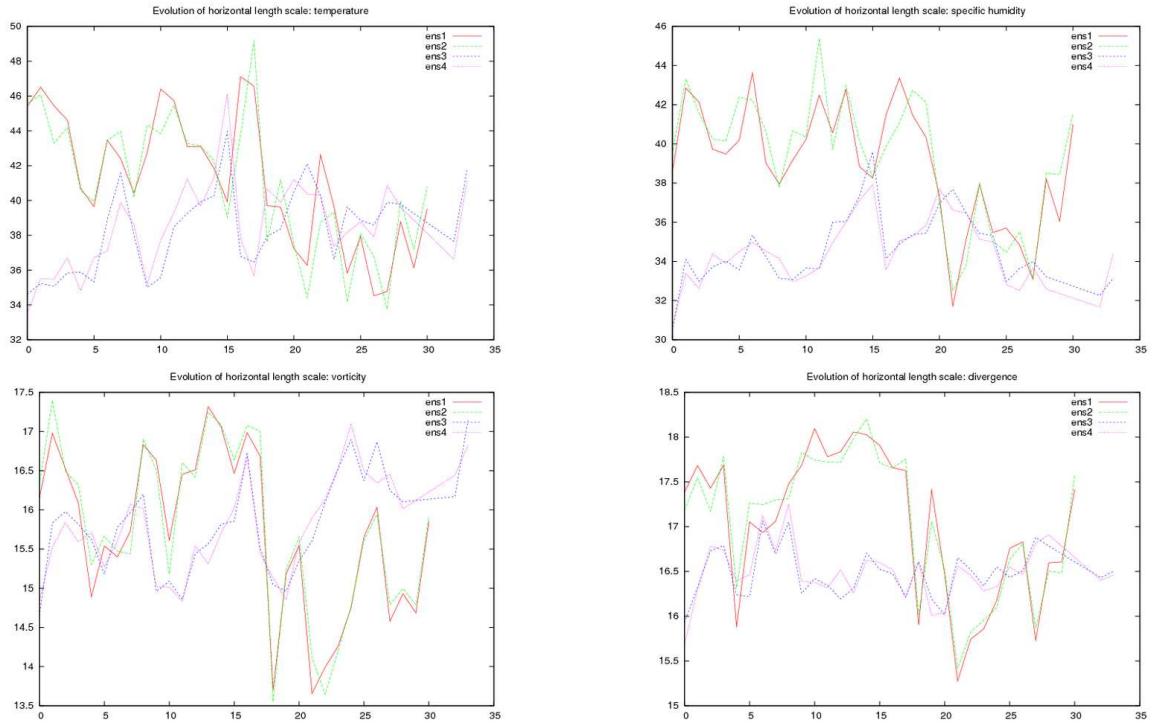

Figure 40: Time evolution of horizontal length-scale for 850hPa at 06UTC: temperature (top left; K), specific humidity (top right; kg kg-1), vorticity (bottom left; Jkg-1 s) and divergence (bottom rigth; s-1); X-axis: number of run days)

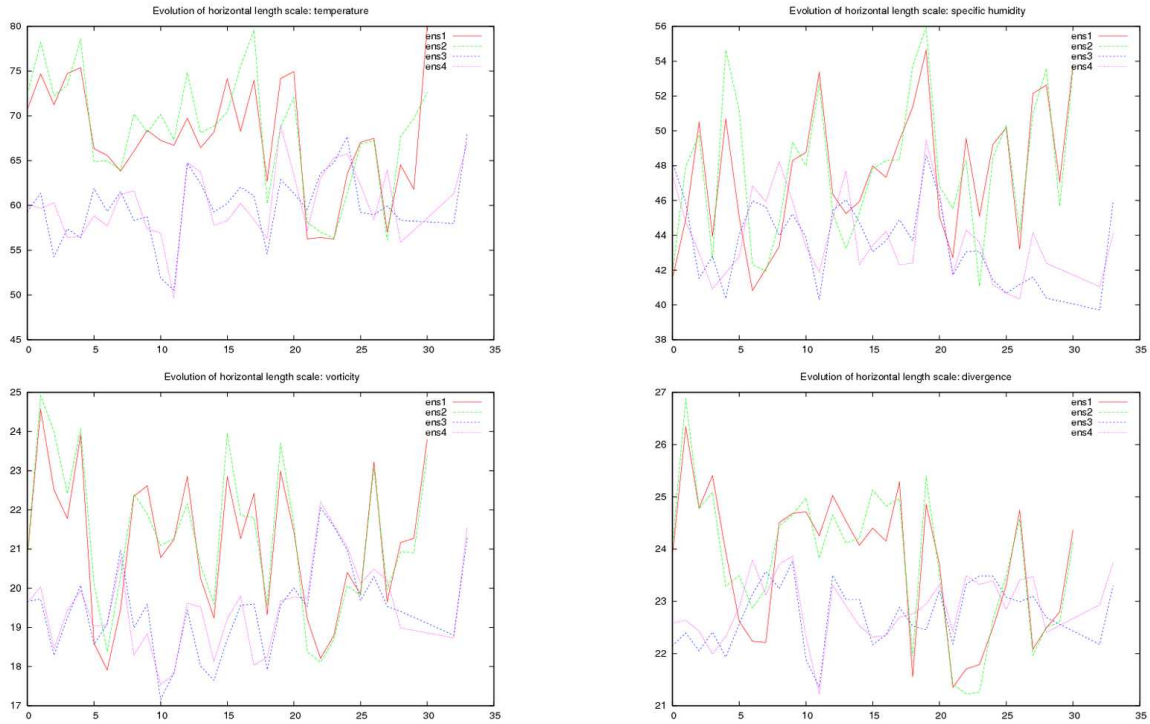

Figure 41: Time evolution of horizontal length-scale for 500hPa at 06UTC: temperature (top left; K), specific humidity (top right; kg kg-1), vorticity (bottom left; Jkg-1 s) and divergence (bottom rigth; s-1); X-axis: number of run days)

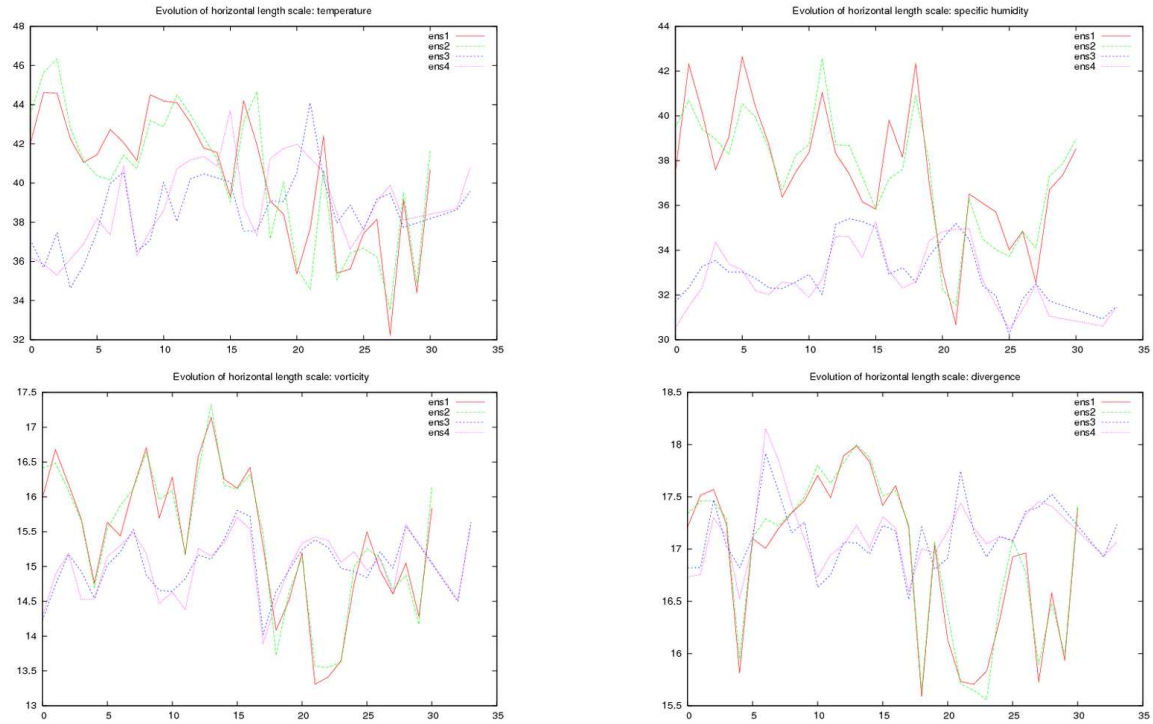

Figure 42: Time evolution of horizontal length-scale for 850hPa at 12UTC: temperature (top left; K), specific humidity (top right; kg kg-1), vorticity (bottom left; Jkg-1 s) and divergence (bottom rigth; s-1); X-axis: number of run days)

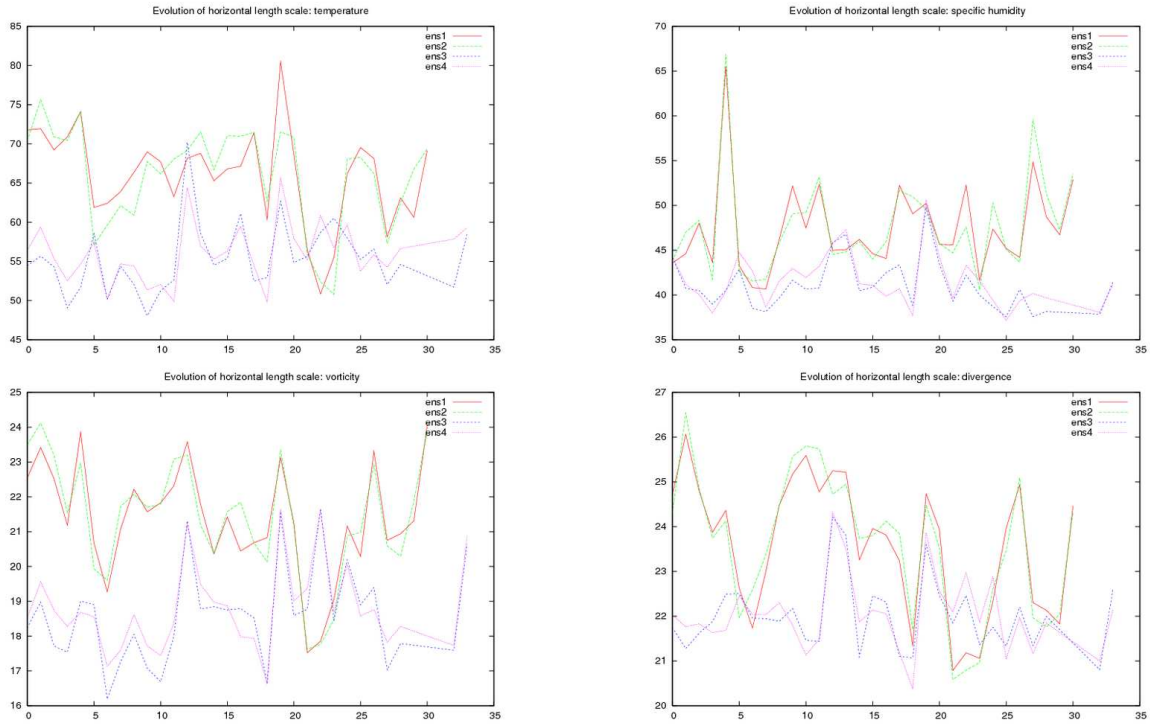

Figure 43: Time evolution of horizontal length-scale for 500hPa at 12UTC: temperature (top left; K), specific humidity (top right; kg kg-1), vorticity (bottom left; Jkg-1 s) and divergence (bottom rigth; s-1); X-axis: number of run days)

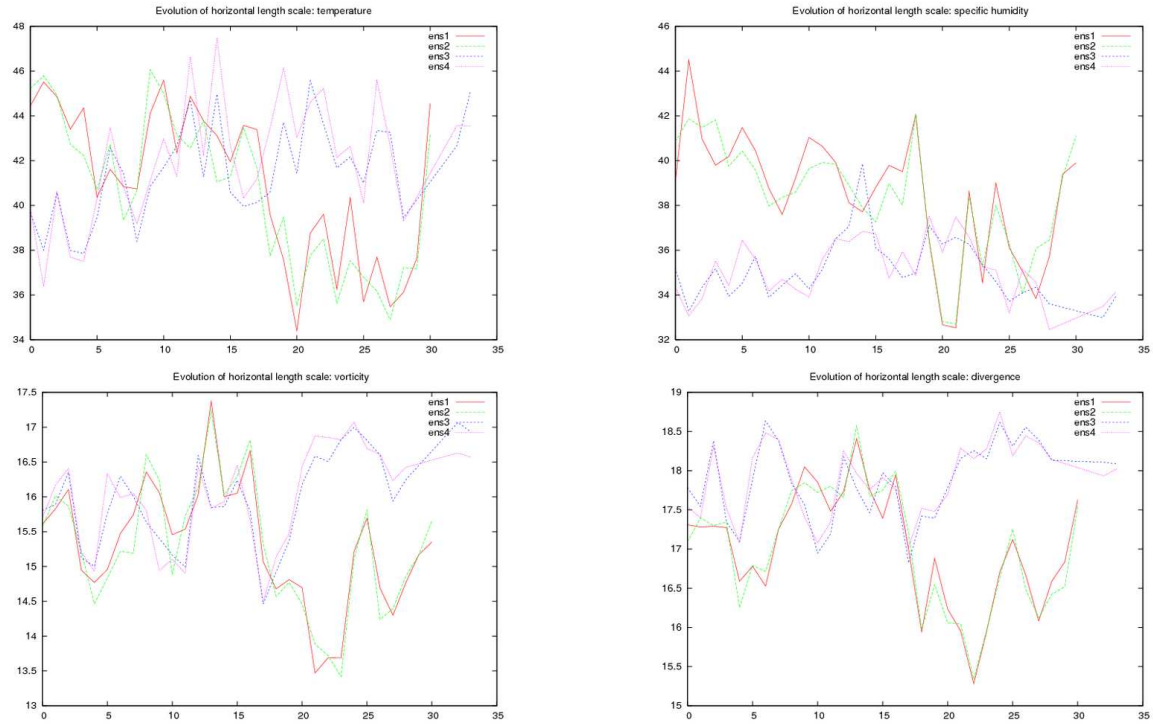

Figure 44: Time evolution of horizontal length-scale for 850hPa at 18UTC: temperature (top left; K), specific humidity (top right; kg kg-1), vorticity (bottom left; Jkg-1 s) and divergence (bottom rigth; s-1); X-axis: number of run days)

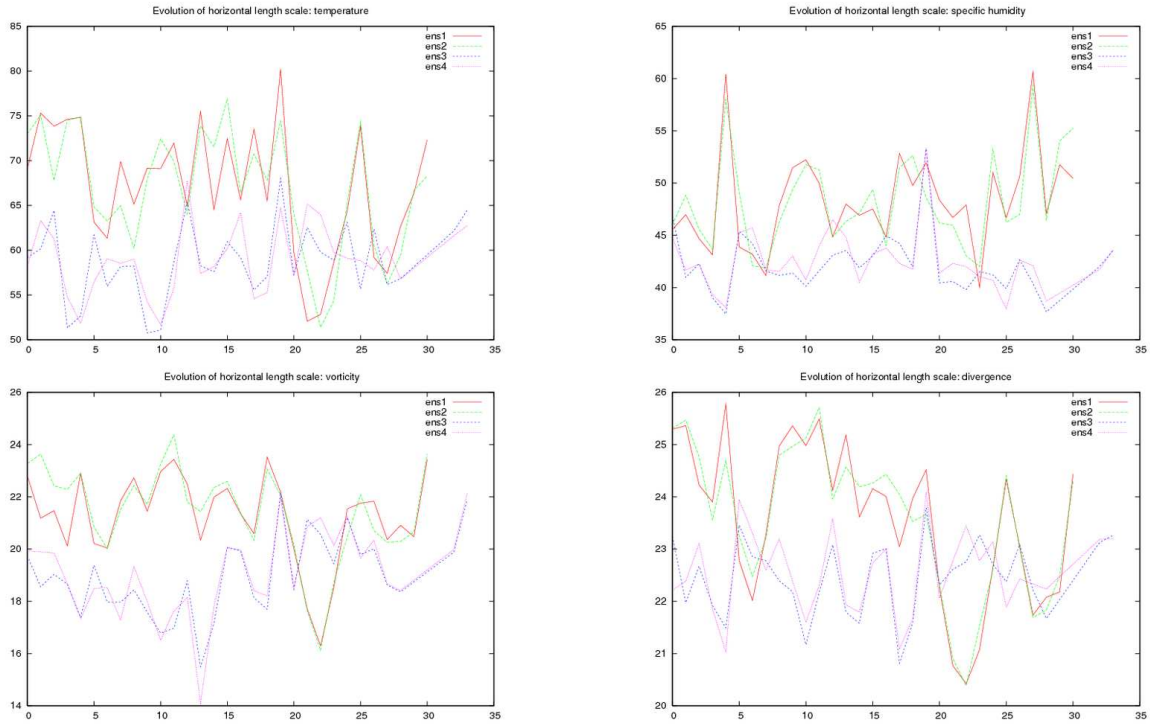

Figure 45: Time evolution of horizontal length-scale for 500hPa at 18UTC: temperature (top left; K), specific humidity (top right; kg kg-1), vorticity (bottom left; Jkg-1 s) and divergence (bottom rigth; s-1); X-axis: number of run days)

C Daily analyse

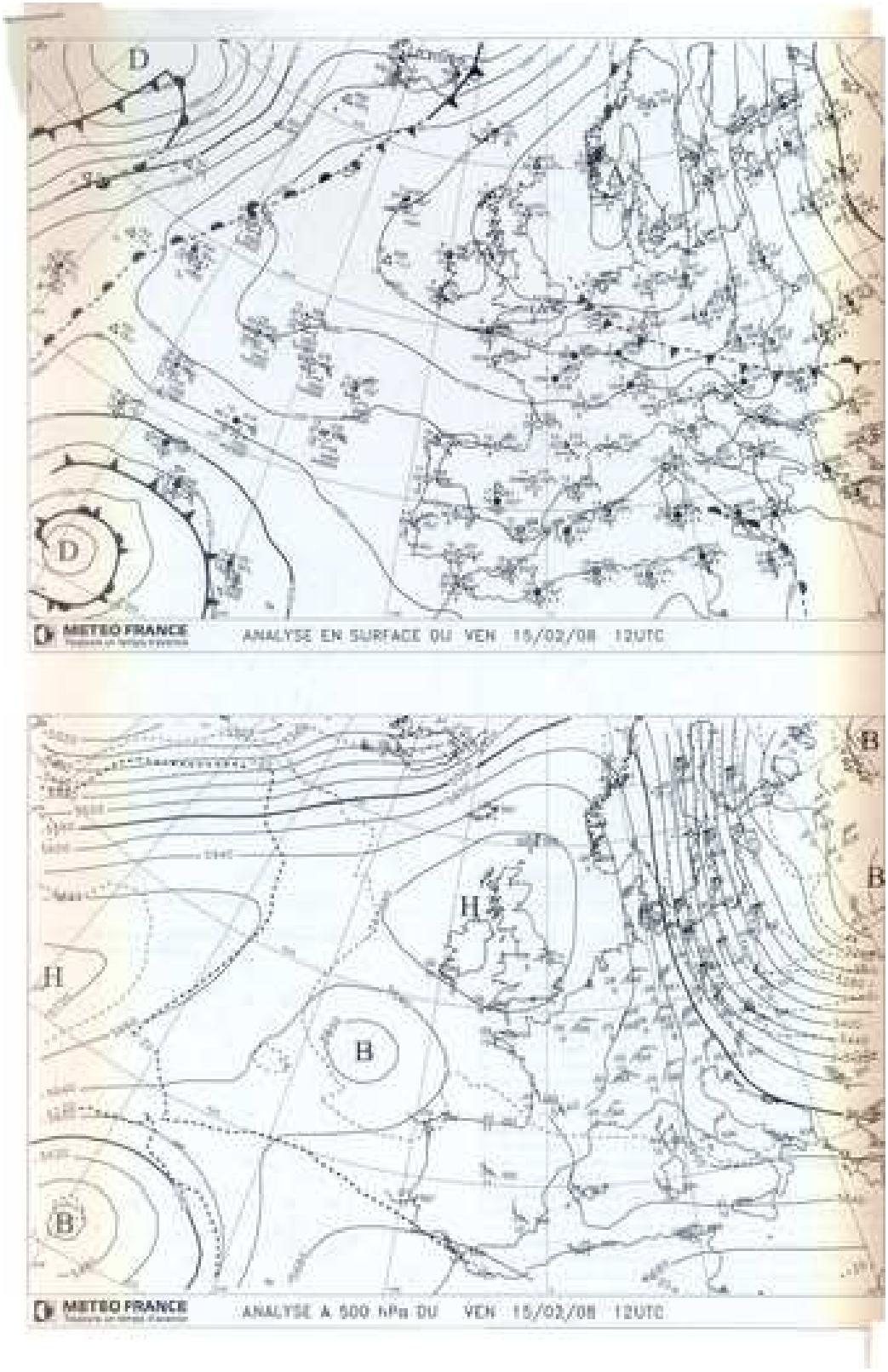

Figure 46: Analyse of the flow on the 15th February 2008

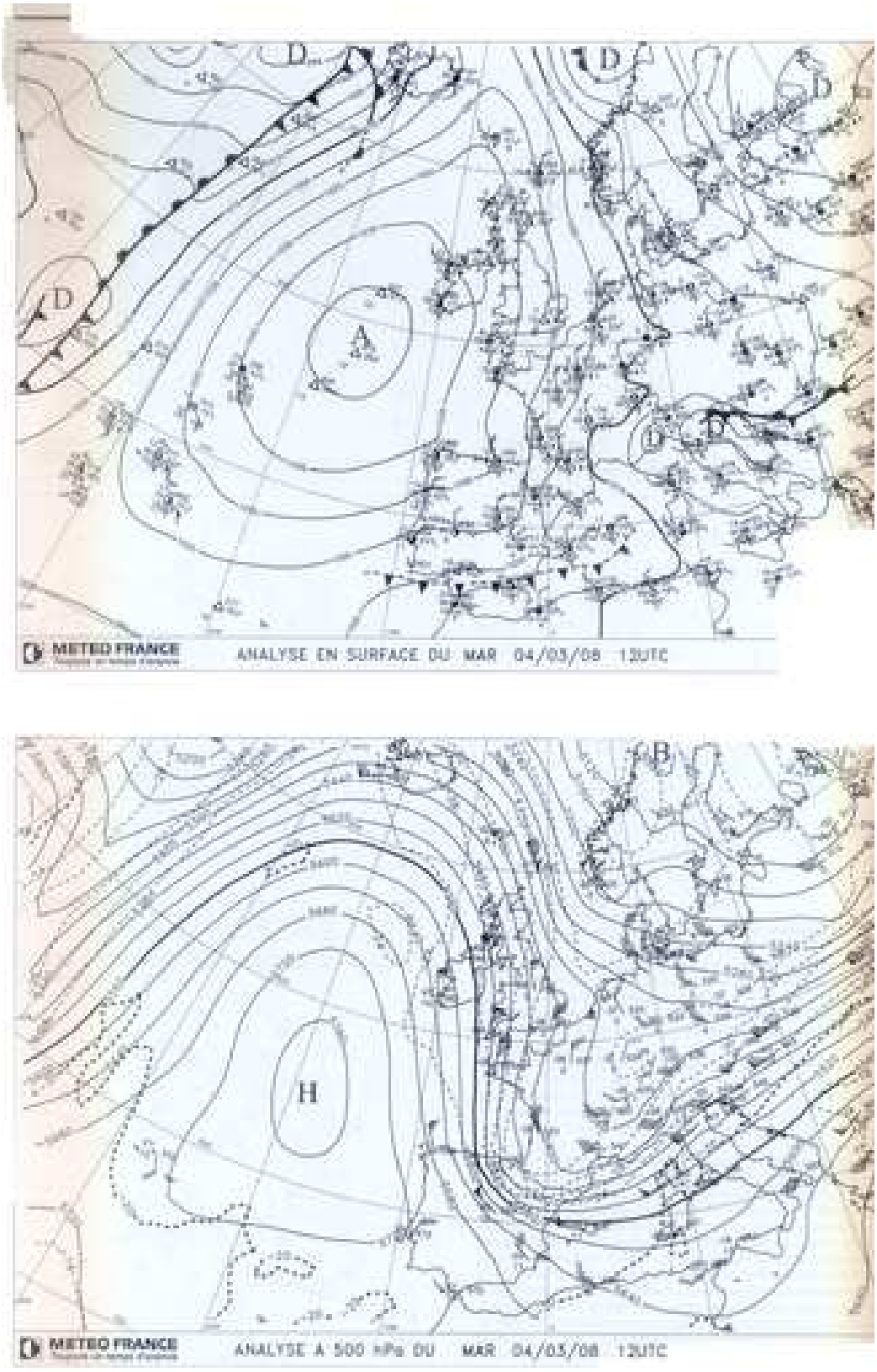

Figure 47: Analyse of the flow on the 4th March 2008